Article

Immunity

The MicroRNA-132 and MicroRNA-212 Cluster Regulates Hematopoietic Stem Cell Maintenance and Survival with Age by Buffering FOXO3 Expression

Highlights

- The miR-212/132 cluster (Mirc19) is enriched in HSCs and upregulated with age
- Mirc19 regulates HSC cycling, function, and survival through autophagy
- Enforced expression or deletion of Mirc19 leads to inappropriate hematopoiesis
- miR-132 directly targets FOXO3 and buffers its expression in aging HSCs

Authors

Arnav Mehta, Jimmy L. Zhao, Nikita Sinha, ..., Aviv Regev, Kamal Chowdhury, David Baltimore

Correspondence

baltimo@caltech.edu

In Brief

Aging hematopoietic stem cells (HSCs) must maintain normal hematopoietic output despite years of replication stress. Baltimore and colleagues show that microRNA-132 helps maintain the balance of HSC survival and normal immune cell production by buffering the transcription factor FOXO3, a known regulator of HSC cycling, function, and survival.

Accession Number

GSE66352

Mehta et al., 2015, Immunity *42*, 1021–1032
June 16, 2015
http://dx.doi.org/10.1016/j.immuni.2015.05.017

CellPress

Immunity
Article

The MicroRNA-132 and MicroRNA-212 Cluster Regulates Hematopoietic Stem Cell Maintenance and Survival with Age by Buffering FOXO3 Expression

Arnav Mehta,[1,2] Jimmy L. Zhao,[1,2] Nikita Sinha,[1] Georgi K. Marinov,[1] Mati Mann,[1] Monika S. Kowalczyk,[3] Rachel P. Galimidi,[1] Xiaomi Du,[1] Erdem Erikci,[5] Aviv Regev,[3,4] Kamal Chowdhury,[5] and David Baltimore[1,*]
[1]Division of Biology and Biological Engineering, California Institute of Technology, Pasadena, CA 91125, USA
[2]David Geffen School of Medicine, University of California, Los Angeles, Los Angeles, CA 90095, USA
[3]The Broad Institute of MIT and Harvard, Cambridge, MA 02142, USA
[4]Department of Biology, Massachusetts Institute of Technology, Cambridge, MA 02140, USA
[5]Department of Molecular Cell Biology, Max Planck Institute of Biophysical Chemistry, Gottingen 37077, Germany
*Correspondence: baltimo@caltech.edu
http://dx.doi.org/10.1016/j.immuni.2015.05.017

SUMMARY

MicroRNAs are critical post-transcriptional regulators of hematopoietic cell-fate decisions, though little remains known about their role in aging hematopoietic stem cells (HSCs). We found that the microRNA-212/132 cluster (Mirc19) is enriched in HSCs and is upregulated during aging. Both overexpression and deletion of microRNAs in this cluster leads to inappropriate hematopoiesis with age. Enforced expression of miR-132 in the bone marrow of mice led to rapid HSC cycling and depletion. A genetic deletion of Mirc19 in mice resulted in HSCs that had altered cycling, function, and survival in response to growth factor starvation. We found that miR-132 exerted its effect on aging HSCs by targeting the transcription factor FOXO3, a known aging associated gene. Our data demonstrate that Mirc19 plays a role in maintaining balanced hematopoietic output by buffering FOXO3 expression. We have thus identified it as a potential target that might play a role in age-related hematopoietic defects.

INTRODUCTION

Hematopoietic stem cells (HSCs) are the source of most all the immune cells in our body (Orkin and Zon, 2008). A complex gene regulatory network tightly regulates the function and survival of HSCs to ensure balanced and appropriate hematopoietic output (Novershtern et al., 2011). Alteration of the HSC niche and deregulation in cell-intrinsic properties such as HSC self-renewal and cycling, metabolism, and survival can have drastic consequences on hematopoietic output (Passegué et al., 2005; Suda et al., 2011). As an organism ages, the balance between HSC self-renewal, function, and survival is drastically altered (Geiger et al., 2013), and this might lead to deleterious consequences such as the inability to effectively combat infection and the onset of autoimmune disease or hematologic cancers (Frasca and Blomberg, 2011; Henry et al., 2011).

Aged HSCs are characterized by increased self-renewal potential, loss of long-term reconstitution capability, myeloid-biased differentiation and a change in niche localization. As a consequence, aged mice demonstrate an accumulation of phenotypically defined HSCs with a poor ability to home to the bone marrow niche (Geiger et al., 2013). These aged HSCs also develop a requirement for basal autophagy for survival, because replication stress and the accumulation of reactive oxygen species have harmful consequences on HSC function with age (Flach et al., 2014; Tothova et al., 2007). The loss of critical autophagic factors is often associated with altered cell cycling of HSCs, and leads to apoptosis and a rapid loss of HSC numbers in aged mice (Miyamoto et al., 2007; Rubinsztein et al., 2011; Warr et al., 2013). A critical balance between cell cycling and differentiation, and survival of aged HSCs must therefore be established to maintain normal hematopoietic output.

Several genetic and epigenetic factors have been identified as important regulators of hematopoietic stem cell aging (Geiger et al., 2013; Rossi et al., 2012; Sun et al., 2014). To date, however, little is known about the role of noncoding RNAs in the regulation of hematopoietic stem cells with age. MicroRNAs, a class of small-noncoding RNAs, are important post-transcriptional regulators of hematopoietic cell-fate decisions (Baltimore et al., 2008; Chen et al., 2004; Gangaraju and Lin, 2009). They alter cell fate by negatively regulating gene expression through direct binding to the 3′untranslated regions of target mRNAs (Filipowicz et al., 2008). Importantly, as post-transcriptional regulators they function to buffer the protein expression of their targets and confer robustness to biological processes such as lineage commitment (Ebert and Sharp, 2012; Mukherji et al., 2011; Strovas et al., 2014).

Several microRNAs have been found to regulate normal function of HSCs, including cell cycling and engraftment potential (Guo et al., 2010; Lechman et al., 2012; Song et al., 2013; Zhao et al., 2013). However, the role of microRNAs in regulating aging HSC function remains unclear. In this work, we studied a previously unappreciated microRNA cluster, Mirc19, that is enriched in HSCs and upregulated with age. These two microRNAs share a seed sequence and therefore target many of the same genes. Several groups have demonstrated that Mirc19 is an important regulator of immune function (Lagos et al., 2010;

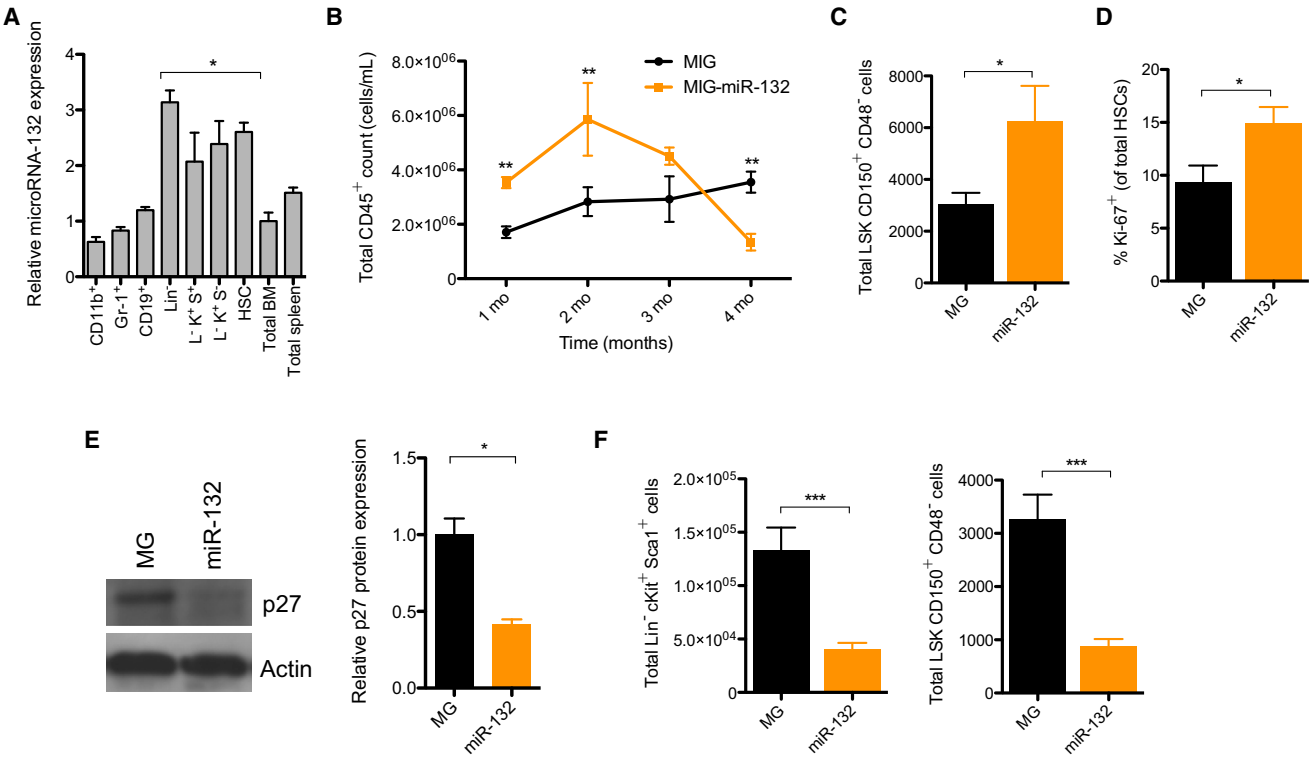

Figure 1. miR-132 Is Expressed in Hematopoietic Stem Cells and Overexpression Alters Hematopoiesis

(A) miR-132 expression in mature and progenitor hematopoietic cells. Cell populations were sorted by flow cytometry directly into RNA lysis buffer and miR-132 expression was detected using TaqMan RT-qPCR (n = 3).

(B–F) WT C57BL/6 mice were lethally irradiated and reconstituted with donor bone marrow cells expressing either a control (MG) or a miR-132 overexpressing (miR-132) retroviral vector (n = 8–12 mice per group). (B) Total numbers of mature leukocytes ($CD45^+$) in the peripheral blood of MG and miR-132 mice at the indicated time points post-reconstitution. (C) Total number of HSCs (LSK $CD150^+$ $CD48^-$) in the bone marrow of MG and miR-132 mice at 8 weeks post-reconstitution. (D) Percentage of Ki-67^+ bone marrow HSCs in MG and miR-132 mice at 8 weeks post-reconstitution. (E) Protein and RNA expression of p27 in the bone marrow of MG and miR-132 mice at 8 weeks post-reconstitution (n = 3). (F) Total number of LSK cells and HSCs in the bone marrow of MG and miR-132 mice at 16 weeks post-reconstitution. Data represent at least three independent experiments and are represented as mean ± SEM. See also Figure S1–S3. * denotes $p < 0.05$, ** denotes $p < 0.01$, and *** denotes $p < 0.001$ using a Student's t test.

Nakahama et al., 2013; Ni et al., 2014; Shaked et al., 2009). We now show that Mirc19 plays a critical role in maintaining the balance between function and survival of aged HSCs. It does this by buffering the expression of its target FOXO3, one of only a few known genes associated with human longevity (Willcox et al., 2008).

RESULTS

Enforced Expression of miR-132 Leads to Depletion of HSCs and Extramedullary Hematopoiesis

To understand the role of the microRNA-212/132 cluster (Mirc19) in hematopoiesis, we first examined the expression of both microRNAs during hematopoietic differentiation. We determined that both miR-132 and miR-212 were enriched in early hematopoietic progenitors ($Lineage^-Sca1^+cKit^+$; LSK cells), and in particular, in long-term hematopoietic stem cells (HSCs: LSK $CD150^+CD48^-$; Figures 1A and S1A). We initially focused on miR-132 because it was the more enriched of the two microRNAs. To investigate the function of miR-132 in these progenitors, we used a retroviral vector to ectopically express miR-132 in hematopoietic stem and progenitor cells (HSPCs) and transferred these miR-132 overexpressing cells into lethally irradiated wild-type (WT) C57BL/6 recipient mice (Figures S1B–S1D). We then monitored mature cell output in the peripheral blood of these mice using flow cytometry to detect the cell-surface markers that identify each cell type. Mice overexpressing miR-132 in the bone marrow compartment ($WT^{miR\text{-}132}$), when compared to empty vector controls (WT^{MG}), demonstrated a rapid accumulation of $CD45^+$ peripheral blood leukocytes at 2 months post-reconstitution, followed by a progressive decline in the number of these cells by 4 months (Figure 1B). A closer inspection of the bone marrow compartment at 2 months post-reconstitution revealed that $WT^{miR\text{-}132}$ mice displayed an expansion in the total number of LSK cells and HSCs (Figure 1C and S1D–S1F). These cells were additionally more proliferative, as measured by the proportion of cells expressing the proliferation marker Ki67, compared to LSK cells and HSCs from age-matched WT^{MG} controls (Figure 1D and S1G). $WT^{miR\text{-}132}$ HSPCs further demonstrated a downregulation in protein and RNA expression of several negative cell cycle regulators, including p27 and p57, although no change in p21 transcript expression

was observed (Figure 1E and S1H). The mRNA expression of p27 remained downregulated in $WT^{miR-132}$ HSPCs compared to WT^{MG} HSPCs at 4 months post-reconstitution (Figure S1I).

We next sought to characterize the cellular basis by which $WT^{miR-132}$ mice undergo depletion in peripheral blood leukocytes at 4 months post-reconstitution. Almost two-thirds (29/44) of the $WT^{miR-132}$ mice presented with gross pathology characteristic of extramedullary hematopoiesis, including enlarged spleens, and a significant elevation of splenic erythtroid cells ($Ter119^+$) (Figures S1J and S1K). None of the age-matched WT^{MG} mice presented such a phenotype and no elevation of myeloid cells was found in the peripheral blood of $WT^{miR-132}$ mice (Figure S1L). Examination of the bone marrow, however, revealed that $WT^{miR-132}$ mice had a severe depletion in the frequency and total number of LSK cells and HSCs compared to WT^{MG} controls (Figure 1F, S1M, and S1N). A similar, more dramatic phenotype was observed at 9 months post-reconstitution in $WT^{miR-132}$ mice (Figure S1O). This phenotype of rapid proliferation followed by depletion of HSCs in the bone marrow compartment is an example of HSC exhaustion.

The depletion of HSCs in $WT^{miR-132}$ mice had the expected dramatic effect on the numbers of more mature progenitor cells, including multi-potent progenitors (MPPs; LSK $CD150^-CD48^+$), lymphoid-primed MPPs (LMPPs; LSK $Flt3^+$), and megakaryocyte and erythroid progenitors (MEPs; $Lineage^-Sca1^-cKit^+CD34^-FcR\gamma^-$). However, no depletion in common myeloid progenitors (CMPs; $Lineage^-Sca1^-cKit^+CD34^+FcR\gamma^-$) or granulocyte-myeloid progenitors (GMPs; $Lineage^-Sca1^-cKit^+CD34^+FcR\gamma^+$) was observed (Figures S1P–S1T). Importantly, the observed alteration in $WT^{miR-132}$ HSCs was intrinsic to the expression of the miR-132 overexpression vector, because no depletion in the proportion of HSCs was evident among the GFP^- cells of $WT^{miR-132}$ and WT^{MG} mice (Figure S1U). Furthermore, we found that the observed phenotype was specific to the expression of authentic miR-132 because overexpression of a miR-132 mutant lacking the correct miR-132 seed sequence resulted in no observable phenotype at 9 months post-reconstitution when compared to WT^{MG} controls (Figure S1V).

We next sought to investigate the role of miR-212 in HSC maintenance. We found that enforced expression of miR-212 in the bone marrow compartment of mice did not result in a significant change in the total number of bone marrow $CD45^+$ cells or LSK cells compared to controls (Figures S1W and S1X). However, we found that there was a significant depletion of HSCs at 4-months post-reconstitution in these mice (Figure S1Y), thus suggesting a less severe phenotype than enforced miR-132 expression, which was consistent with the lower amounts of enrichment of miR-212 in HSCs.

Mirc19 Has a Physiological Role of Protecting the Aging Hematopoietic System

To determine whether miR-132 has a physiological role in regulating hematopoietic stem cell function, we obtained mice that have a genetic deletion in both of the microRNAs in the Mirc19 cluster (*Mirc19*$^{-/-}$) (Ucar et al., 2012). We observed no apparent defect in the output of mature hematopoietic cells in the peripheral blood, spleen, and bone marrow of 12-week-old *Mirc19*$^{-/-}$ mice when compared to age-matched wild-type (WT) controls (Figures S2A–S2D). We noticed, however, an upregulation of miR-132 expression in the bone marrow and LSK compartment of aged (2-year-old) WT mice compared to young (12-week-old) WT mice (Figure 2A), and posited a more important role of miR-132 in maintaining the fidelity of aging HSCs. Consistent with this, we found that unlike in 12-week-old mice (Figure S2D), aged (60-week-old) *Mirc19*$^{-/-}$ mice had an elevation in the total number of HSCs (LSK $CD150^+CD48^-$ and LSK $EPCR^+$) in the bone marrow compartment compared to WT controls (Figure 2B). Surprisingly, this was accompanied by a decrease in the total number of bone marrow LSK cells, which are mostly downstream products of HSCs (Figure 2B). Aged *Mirc19*$^{-/-}$ mice further presented with enlarged spleens (Figure S2E) and a global depletion of all major mature cell types in the bone marrow compartment (Figure S2F), indicative of a failure of HSCs to maintain normal hematopoietic output and the onset of extramedullary hematopoiesis.

To investigate the molecular basis for the role of Mirc19 in HSCs, we performed gene expression analysis by bulk population RNA-sequencing on WT and *Mirc19*$^{-/-}$ long-term HSCs (LSK $CD150^+CD48^-$), short-term HSCs (LSK $CD150^-CD48^-$), and multipotent progenitors (LSK $CD150^-CD48^+$). Approximately 14,000 genes were expressed in each sample (Figure S2N), and clustering based on the number differentially expressed genes revealed close similarity between WT short-term and long-term HSC subsets and *Mirc19*$^{-/-}$ short-term and long-term HSC subsets, with both these groups differing significantly from the MPP populations (Figure 2C). Differentially expressed genes between the WT and *Mirc19*$^{-/-}$ HSC populations were enriched for several functional annotations relevant to HSC biology, including regulation of cell-cycle, cell differentiation, response to stress, and cell death (Figure 2D).

To investigate whether the observed phenotype in *Mirc19*$^{-/-}$ mice is intrinsic to the hematopoietic system, we transferred bone marrow cells from 12-week-old WT or *Mirc19*$^{-/-}$ mice into irradiated WT recipients. After 1 year, the phenotypes in transplanted mice closely resembled that of aged WT and *Mirc19*$^{-/-}$ mice, respectively, consistent with a defect intrinsic to the hematopoietic system (Figure S2G). We employed an inflammatory model for hematopoietic aging (Esplin et al., 2011) to determine whether this was sufficient to recreate the observed alteration in hematopoiesis. We delivered LPS nine times over 1 month to 16-week-old *Mirc19*$^{-/-}$ and WT mice. We found that, consistent with the altered hematopoietic output we observed in aged mice, *Mirc19*$^{-/-}$ mice presented with severely enlarged spleens containing an enrichment of splenic HSCs compared to WT mice also injected with LPS (Figures 3A and S2H). Similar to aged *Mirc19*$^{-/-}$ mice, LPS-treated *Mirc19*$^{-/-}$ mice also demonstrated an accumulation of HSCs and a decrease in the frequency of LSK cells in the bone marrow compartment compared to LPS treated WT controls (Figure 3B). This skewing of hematopoietic progenitor output in *Mirc19*$^{-/-}$ mice might be characterized by an increase in the total number of long-term HSCs and a reduction in total number of short-term HSCs and MPPs in the bone marrow compartment (Figure S2I). We can therefore mimic the aging-related hematopoietic defect observed in *Mirc19*$^{-/-}$ by exposing younger mice to chronic inflammatory stimuli via repetitive LPS injections.

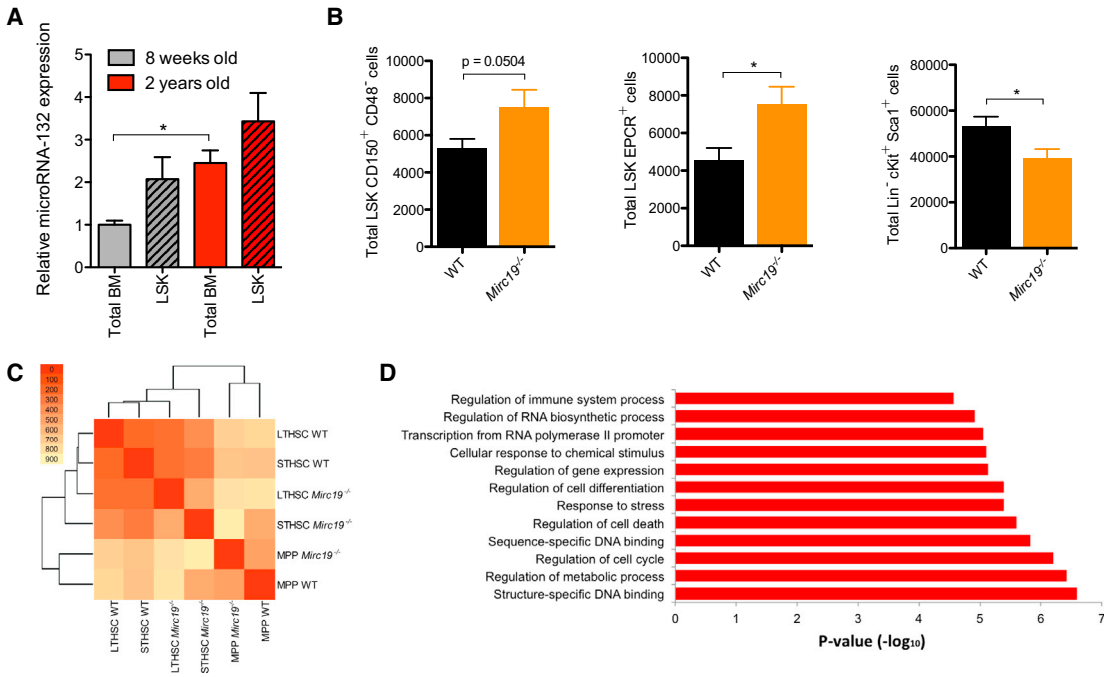

Figure 2. Genetic Deletion of *Mirc19* in Mice Alters Hematopoietic Output with Age

(A) miR-132 expression in total bone marrow and LSK cells from 8-week-old and 2-year-old C57BL/6 WT mice. miR-132 expression was quantified by TaqMan RT-qPCR (n = 2).

(B–D) Mice with a genetic deletion of *Mirc19* (*Mirc19*$^{-/-}$) along with WT mice in the C57BL/6 background were analyzed. (B) Total number of HSCs (LSK CD150^{+} CD48^{-} and LSK EPCR^{+}) and LSK cells in the bone marrow compartment of 60- to 64-week-old WT and *Mirc19*$^{-/-}$ mice (n = 7–12 mice per group). (C) Global expression profiling of WT and *Mirc19*$^{-/-}$ HSCs, as well as short-term HSCs and MPPs, from 16-week-old mice using RNA-seq. The heat map represents the number of differentially expressed genes between the different WT and *Mirc19*$^{-/-}$ populations. (D) Enriched gene-ontology terms for differently expressed genes between WT and *Mirc19*$^{-/-}$ progenitors. Data represent at least two independent experiments and are represented as mean ± SEM. See also Figures S4–S6. * denotes $p < 0.05$, ** denotes $p < 0.01$, and *** denotes $p < 0.001$ using a Student's t test.

Loss of Mirc19 Reduces HSC Cycling and Improves Engraftment Potential

The cycling characteristics of HSCs are closely related to their ability to self-renew and differentiate into committed progenitors (Pietras et al., 2011). Furthermore, increased HSC quiescence and an increase in HSC number is characteristic of the aging hematopoietic system (Geiger et al., 2013). We thus sought to determine whether the accumulation of HSCs and decrease in output of more committed progenitors in *Mirc19*$^{-/-}$ mice might be a result of altered cell cycling. We performed cell-cycling analysis using flow cytometry by staining for the proliferation marker Ki67 and utilizing the dsDNA dye Hoescht33342. Under steady-state conditions, we observed no major defect in cell cycling in 16-week-old *Mirc19*$^{-/-}$ mice compared to age-matched WT mice (Figure S2J). However, under conditions of inflammatory stress such as low-grade LPS stimulation, we found that *Mirc19*$^{-/-}$ HSCs were far less proliferative, with an almost 50% increase in the number of cells in the G_0 phase of the cell cycle compared to WT HSCs (Figures 3C–3E). Importantly, we observed a substantial decrease in the number of HSCs in G_1 and only a small proportion of cells in S/M phases of the cell cycle in *Mirc19*$^{-/-}$ mice (Figures 3C–3E). No change in p27 mRNA expression was observed at steady state between *Mirc19*$^{-/-}$ and WT HSCs. However, in mice treated with either LPS or 5-fluorouracil, which induce HSC proliferation, the expression of p27 in the bone marrow compartment was upregulated in *Mirc19*$^{-/-}$ mice compared to WT mice (Figures S2K and S2L). It therefore follows that the loss of Mirc19 leads to increased HSC quiescence and an accumulation of HSCs, with a concomitant decrease in the number of more committed progenitors.

The majority of HSCs in the hematopoietic system remain in a dormant state, and disruption of this quiescence can have serious consequences for HSC function (Rossi et al., 2012). To investigate whether the alteration in cell cycling of aged *Mirc19*$^{-/-}$ HSCs might be related to altered HSC function, we performed competitive transplant assays. Aged (60 weeks) CD45.2 *Mirc19*$^{-/-}$ or WT HSCs were transplanted with equal numbers of CD45.1 WT HSCs into lethally irradiated CD45.2 recipient mice. The peripheral blood of these mice was analyzed at 4 months post-reconstitution for repopulation of major mature cell types. The cells from aged *Mirc19*$^{-/-}$ mice were more effective at reconstituting most all immune cells than those from aged WT mice, evidenced in total blood leukocytes (CD45^{+}), B cells (CD19^{+}), myeloid cells (CD11b^{+}), and granulocytes (Gr-1^{+}) in the peripheral blood (Figure 4A). An insignificant difference in the relative proportion of T cells (CD3ε^{+}) was observed (Figure 4A). Competitive transplant of young (12 weeks) *Mirc19*$^{-/-}$ HSCs yielded no observable functional difference compared to young WT HSCs except for defective repopulation of T cells (Figure 4B); however,

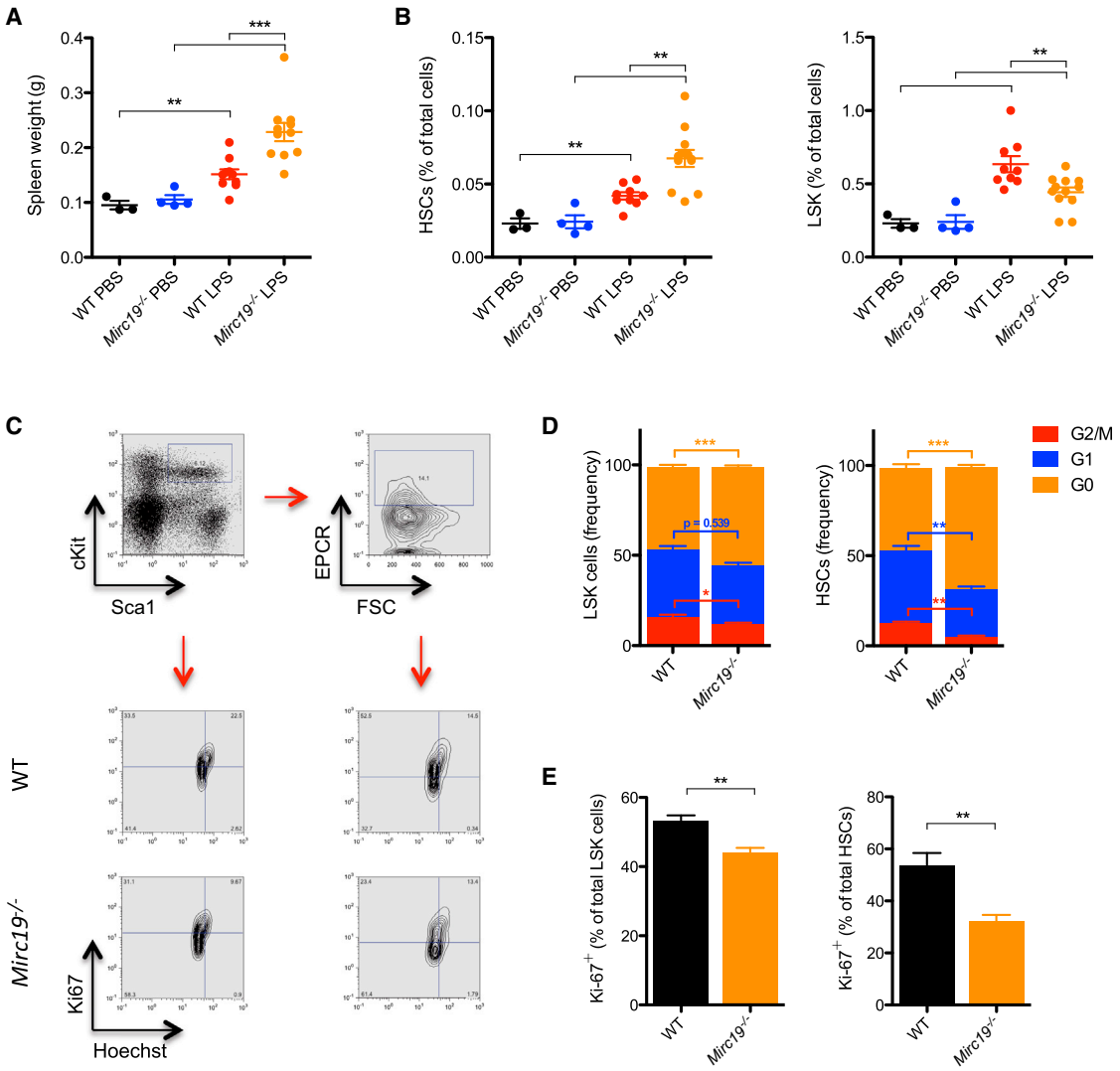

Figure 3. Genetic Deletion of *Mirc19* in Mice Alters Hematopoietic Output and Cycling in Response to LPS Stimulation

(A–E) 6-month-old WT and *Mirc19*$^{-/-}$ mice were treated with nine evenly-spaced low-dose (1 mg/kg of body weight) LPS or PBS injections over one month. (A) Spleen weights of WT and *Mirc19*$^{-/-}$ mice treated with PBS or LPS. (B) Proportion of HSCs and LSK cells within the bone marrow compartment of WT and *Mirc19*$^{-/-}$ mice treated with LPS or PBS. (C) Representative flow-cytometry plots for cell-cycle analysis of HSCs and LSK cells from WT and *Mirc19*$^{-/-}$ mice following LPS injection. (D) Proportion of bone marrow LSK cells and HSCs in each stage of the cell cycle (G0, G1, G2/M) from WT and *Mirc19*$^{-/-}$ mice following LPS injection. (E) Proportion of bone marrow LSK cells and HSCs expressing Ki67 from WT and *Mirc19*$^{-/-}$ mice following LPS injection. Data represent at least two independent experiments and are represented as mean ± SEM. See also Figures S4 and S5. * denotes $p < 0.05$, ** denotes $p < 0.01$, and *** denotes $p < 0.001$ using a Student's t test.

secondary transplantation of young *Mirc19*$^{-/-}$ HSCs yielded a similar phenotype to that observed with primary transplantation of aged *Mirc19*$^{-/-}$ HSCs (Figure S2M). Consistent with the increased quiescence of aged *Mirc19*$^{-/-}$ HSCs compared to WT HSCs, *Mirc19*$^{-/-}$ cells performed better at long-term repopulation. Additionally, HSCs obtained from WT$^{miR-132}$ mice, which ectopically overexpressed miR-132, were severely defective in long-term reconstitution in competitive transplant assays compared to control HSCs obtained from WT^{MG} mice (Figure 4C). It therefore appears that Mirc19 is important for tuning the interplay between quiescence and functional output of the aging hematopoietic system.

FOXO3 Is a Target of miR-132 in Bone Marrow Cells

To understand the molecular mechanism of miR-132 action, we characterized the expression of the best computationally predicted targets of miR-132 from TargetScan under conditions of miR-132 overexpression (Friedman et al., 2009). RNA was extracted from lineage-depleted bone marrow cells of WT$^{miR-132}$ and WT^{MG} mice and was subjected to quantitative PCR (qPCR) for target genes relevant to HSC function. The most significantly downregulated targets under conditions of ectopic expression of miR-132 in WT$^{miR-132}$ bone marrow, relative to control WT^{MG} bone marrow, were pursued for further analysis. Messenger RNA expression of several genes relevant to

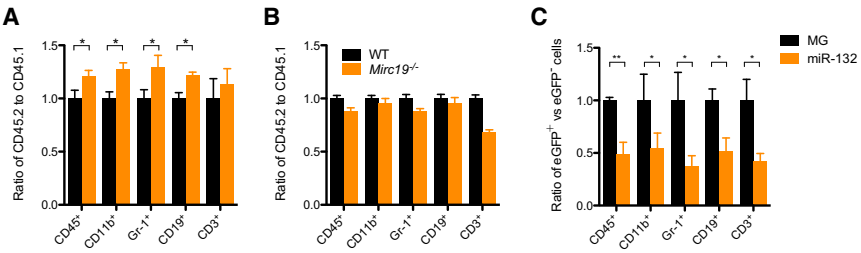

Figure 4. Mirc19 Regulates Long-Term Reconstitution Potential of HSCs with Age

(A and B) WT or *Mirc19*$^{-/-}$ CD45.2$^+$ bone marrow cells, calibrated for the total number of phenotypically defined HSCs, were injected in a 1:1 ratio with CD45.1$^+$ WT bone marrow cells into irradiated C57BL/6 CD45.2$^+$ recipients. (A) Ratio of total CD45.2$^+$ cells to CD45.1$^+$ cells at 16 weeks post-reconstitution for various mature immune cell types in the peripheral blood of mice injected with aged WT and *Mirc19*$^{-/-}$ CD45.2$^+$ cells. Data was normalized to proportion of WT CD45.2$^+$ cells. (B) Ratio of total CD45.2$^+$ cells to CD45.1$^+$ cells at 16 weeks post-reconstitution for various mature immune cell types in the peripheral blood of mice injected with young WT and *Mirc19*$^{-/-}$ CD45.2$^+$ cells.

(C) Control (MG) or miR-132 overexpressing (miR-132) bone marrow HSCs, both expressing a retroviral vector containing eGFP, were injected in a 1:1 ratio with un-infected WT bone marrow HSCs into irradiated C57BL/6 mice. Graphs show the ratio of eGFP$^+$ cells to eGFP$^-$ cells for various immune cell types in the peripheral blood of recipients at 16 weeks post-reconstitution. Data represent two independent experiments and are represented as mean ± SEM. * denotes $p < 0.05$ using a Student's t test.

hematopoiesis was downregulated in WT$^{miR\text{-}132}$ bone marrow samples including AchE, FOXO3, Lin28B, MMP9, and SOX4 (Figure 5A). We sought to further investigate the role of FOXO3 in mediating the effect of miR-132 on HSCs because it contains a perfect 8-mer binding site for miR-132 (Figure 5B) and is the most significantly downregulated of these genes. Importantly, we also found a global upregulation of miR-132 targets in our RNA-sequencing analysis of *Mirc19*$^{-/-}$ and WT HSCs, and this included an upregulation of FOXO3 transcript expression, as well as some of its downstream targets (Figures S2O–S2Q). We validated that miR-132 binds directly to the FOXO3 3′-untranslated region (3′UTR) using a luciferase reporter assay in which the FOXO3 3′UTR was expressed immediately downstream of luciferase. We found that in the presence of miR-132, the expression of this reporter was significantly lower than from a vector lacking the FOXO3 3′UTR (Figure 5C). This binding was specific to miR-132 because mutating the miR-132 binding site on the FOXO3 3′UTR normalized luciferase expression (Figure 5C).

We next quantified FOXO3 protein expression in bone marrow cells from WT$^{miR\text{-}132}$ and WT^{MG} mice. Consistent with FOXO3 being a target of miR-132, we found protein expression was significantly downregulated in WT$^{miR\text{-}132}$ mice compared to WT^{MG} mice (Figure 5D). Expression of FOXO1 and FOXO4, closely related family members of FOXO3, remained unchanged in WT$^{miR\text{-}132}$ bone marrow cells (Figure S3A). Importantly, we also found that FOXO3 mRNA and protein expression was elevated in lineage-depleted bone marrow cells from *Mirc19*$^{-/-}$ mice compared to WT controls (Figures 5E and 5F). Expression of FOXO4 was also slightly elevated in *Mirc19*$^{-/-}$ cells and expression of FOXO1 was unchanged (Figure S3B). We additionally performed intracellular staining of FOXO3 and phospho-FOXO3 (p-FOXO3) protein. As expected, we found elevated protein expression of FOXO3 in *Mirc19*$^{-/-}$ HSCs compared to WT controls. However, we saw only a marginal elevation in p-FOXO3 in *Mirc19*$^{-/-}$ HSCs, indicating that the majority of extra FOXO3 in these cells is likely in the nucleus in its active, un-phosphorylated state (Figures S3C and S3D). Together, the data indicate that miR-132 is an important regulator of FOXO3 expression in bone marrow cells. As was observed with miR-132 expression, FOXO3 mRNA expression was increased in bone marrow cells from aged mice compared to those of young mice (Figure 6A), thus suggesting that miR-132 might serve to maintain FOXO3 protein expression within a balanced range for normal hematopoietic function.

miR-132 Regulates HSC Cycling and Function through FOXO3

To determine whether FOXO3 is a key mediator of miR-132 function, we co-expressed FOXO3 with miR-132 in the bone marrow compartment of WT mice to see whether it would rescue the phenotype observed with miR-132 expression alone. FOXO3 cDNA lacking a miR-132 target site was cloned into the MSCV-IRES-eGFP (MIG) vector immediately downstream of the MSCV promoter (Figure 6B). As previously described, miR-132 was cloned downstream of eGFP. Lethally irradiated mice were reconstituted with bone marrow cells transduced with a control vector (WT^{MIG}) or a vector expressing both miR-132 and FOXO3 (WT$^{FOXO3+miR\text{-}132}$), miR-132 only (WT$^{miR\text{-}132}$), or FOXO3 only (WT^{FOXO3}). The expression of miR-132 and FOXO3 was validated by qPCR and Immunoblot, respectively (Figures S3E and S3F). We observed the mean fluorescence intensity of eGFP in bone marrow cells expressing only FOXO3 to be lower than that of the other vectors, suggesting that overexpression of FOXO3 above endogenous concentrations might be toxic (Figure S3G). We additionally observed that a larger fraction bone marrow HSCs from WT^{FOXO3} mice expressed AnnexinV compared to WT^{MIG} controls (Figure S3H). This effect was not observed when FOXO3 was co-expressed with miR-132, presumably because baseline expression of FOXO3 was already downregulated due to miR-132 overexpression.

As expected, a reduction in peripheral blood leukocytes was observed in WT$^{miR\text{-}132}$ mice compared to WT^{MIG} mice at 4-months post-reconstitution (Figure 6C). Co-expression of FOXO3 with miR-132, however, rescued this defect, because no significant change in peripheral blood leukocytes was observed in WT$^{FOXO3+miR\text{-}132}$ mice compared to WT^{MIG} controls (Figure 6C). Examination of the bone marrow compartment of WT$^{FOXO3\ +\ miR\text{-}132}$ mice revealed total numbers of HSCs and LSK cells comparable to WT^{MIG} controls, demonstrating a rescue of HSC depletion observed with the expression of miR-132 alone (Figures 6D and 6E). In addition, expression of FOXO3 alone resulted in a moderate elevation in the total number of bone marrow LSK cells compared to control mice (Figure 6E). HSCs from WT$^{FOXO3+miR\text{-}132}$ mice also showed comparable proportions of Ki67 staining to HSCs from WT^{MIG} mice,

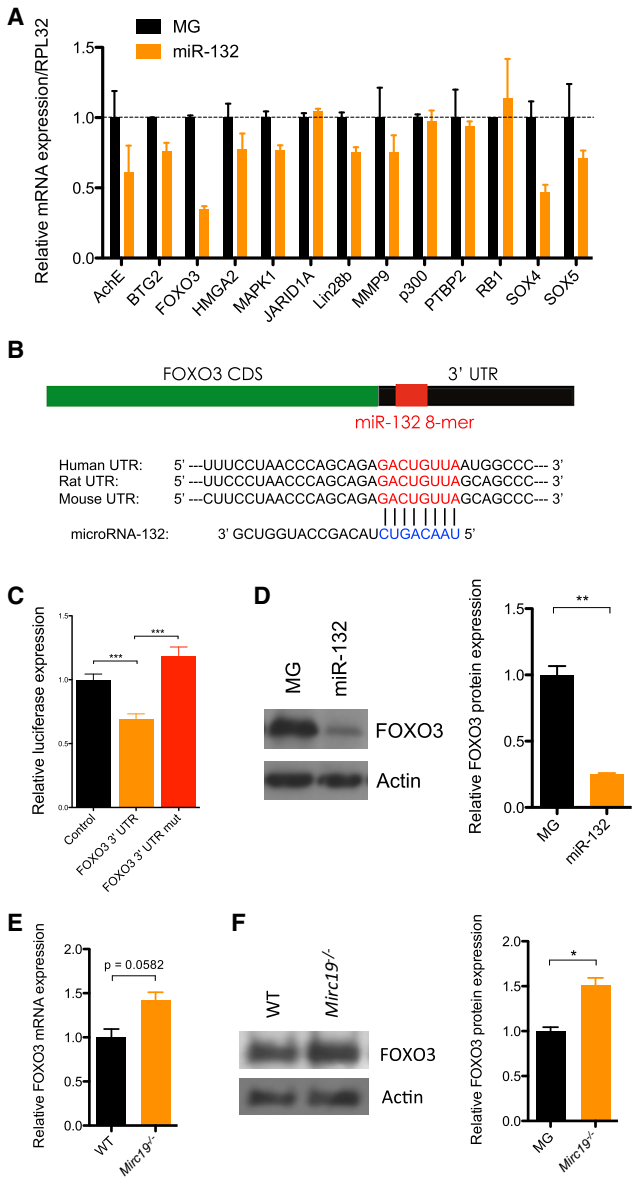

Figure 5. FOXO3 Is a Direct Target of miR-132 in Bone Marrow Cells

(A) mRNA expression by RT-qPCR of computationally predicted miR-132 targets in control (MG) or miR-132 overexpressing (miR-132) bone marrow cells.

(B) Schematic of the predicted miR-132 binding site in the FOXO3 3′UTR.

(C) Relative luciferase expression in 293T cells transfected with a miR-132 overexpression vector and either a vector containing luciferase only (control), a vector containing luciferase and the FOXO3 3′UTR immediately downstream (FOXO3 3′UTR), or a vector containing luciferase and a FOXO3 3′UTR with a mutated miR-132 binding site (FOXO3 3′UTR mut).

(D) FOXO3 protein expression in bone marrow cells from MG and miR-132 mice obtained by Western blot.

(E) FOXO3 transcript expression in lineage-depleted bone marrow cells obtained from WT or miR-212/132$^{-/-}$ mice.

(F) FOXO3 protein expression in lineage-depleted bone marrow cells obtained from WT or *Mirc19*$^{-/-}$ mice. See also Figures S7A–S7C. Data represents at least two independent experiments (n = 2) and is represented as mean ± SEM. * denotes $p < 0.05$, ** denotes $p < 0.01$, and *** denotes $p < 0.001$ using a Student's t test.

indicating that these cells were not prone to cycling like WT$^{miR-132}$ cells (Figure 5F). WT^{FOXO3} HSCs demonstrated a significant albeit moderate decrease in the proportion of cycling HSCs compared to controls (Figure 6F). These experiments suggest that co-expression of FOXO3 can rescue the phenotype observed with expression of miR-132 alone. It seems likely that miR-132 regulates hematopoiesis primarily by directly modulating FOXO3 protein expression, although we cannot rule out that FOXO3 overexpression is able to override the miR-132 effect while the true targets of miR-132 in the bone marrow are other genes.

Loss of Mirc19 Affects HSC Survival through Protective Autophagy

FOXO3 is critical for maintaining the hematopoietic stem cell pool by regulating HSC cell-cycling and resistance to oxidative stress (Miyamoto et al., 2007; Tothova et al., 2007). It is also implicated in maintaining the survival of aging HSCs by directing protective autophagy (Warr et al., 2013). To this end, we found that several autophagy-related genes were upregulated in *Mirc19*$^{-/-}$ HSCs compared to WT controls upon inspection of our RNA-sequencing dataset (Figure S2R). Thus, to determine whether miR-132 might play a role in altering survival of HSCs, we sorted HSCs from WT and *Mirc19*$^{-/-}$ mice and cultured them in the presence or absence of survival growth factors and cytokines including mouse stem cell factor (mSCF), mouse interleukin-6 (mIL-6), mIL-3, TPO, and Flt3L. We used a luciferase-based assay to monitor caspase activity after 12 hr in culture. In the presence of survival factors, minimal activity was observed in both WT and *Mirc19*$^{-/-}$ HSCs. However, under starvation conditions, which induces protective autophagy in aged HSCs (Warr et al., 2013), *Mirc19*$^{-/-}$ HSCs demonstrated a significant reduction in induction of apoptosis compared to WT HSCs (Figure 7A). This is consistent with the more rapid induction of a protective autophagy program due to higher expression of FOXO3 in *Mirc19*$^{-/-}$ HSCs. Importantly, when autophagy was inhibited by Bafilomycin A (BafA), a known inhibitor of autophagosome fusion to lysosomes, *Mirc19*$^{-/-}$ and WT HSCs underwent comparable, higher amounts of apoptosis (Figure 7A). As previously reported, FOXO3 expression had no major effect on autophagy and apoptosis of myeloid progenitors (Figure 7B).

To determine whether *Mirc19*$^{-/-}$ HSCs indeed induce the autophagy machinery more potently than WT HSCs, we utilized a fluorescent reporter for autophagosome formation that was detectable by flow cytometry. The efficacy of this assay in detecting autophagosome formation was validated by comparing signal intensity in WT cells to autophagy deficient cells (Figure S3I). WT and *Mirc19*$^{-/-}$ HSCs were cultured under growth-factor rich or starvation conditions as described above and were stained for the presence of autophagosomes. Under starvation conditions, *Mirc19*$^{-/-}$ HSCs demonstrated higher amounts of autophagosome formation compared WT HSCs (Figure 7C). In the presence of LY2940002, a PI3-kinase inhibitor and early inhibitor of autophagy, autophagosome formation was decreased to comparable amounts in *Mirc19*$^{-/-}$ and WT HSCs (Figure 7C). We additionally sought to investigate whether the potent induction of autophagy in *Mirc19*$^{-/-}$ HSCs may improve survival by altering reactive-oxygen species (ROS) accumulation. We utilized a fluorescent detection system for ROS and

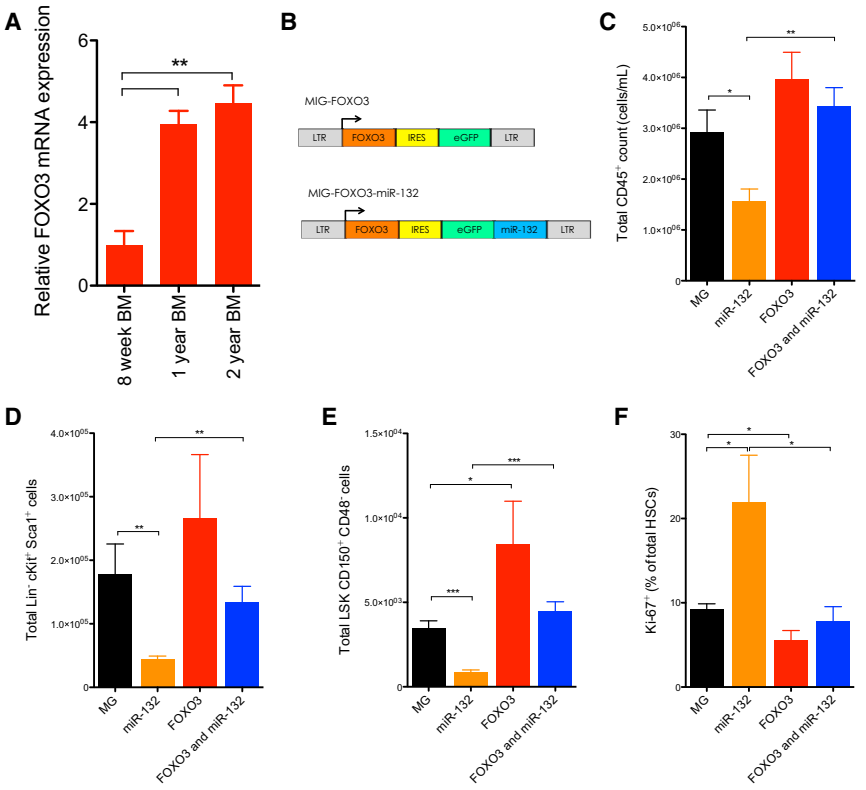

Figure 6. Co-expression of FOXO3 with miR-132 Rescues the Hematopoietic Defects Observed with Expression of miR-132 Alone

(A) FOXO3 mRNA expression by RT-qPCR in total bone marrow cells from 8-week-old, 1-year-old, and 2-year-old C57BL/6 WT mice (n = 2).

(B) Schematic of retroviral vectors constructed for expression of FOXO3 only or for co-expression of FOXO3 along with miR-132.

(C–F) WT C57BL/6 mice were lethally irradiated and reconstituted with donor bone marrow cells expressing either a control (MG), a miR-132-over-expressing (miR-132), a FOXO3-overexpressing (FOXO3), or a FOXO3- and miR-132-over-expressing (FOXO3 and miR-132) retroviral vector (n = 10–12 mice per group). (C) Total peripheral blood $CD45^+$ leukocytes in the respective animals at 16 weeks post-reconstitution. (D) Total LSK cells in the bone marrow compartment of the respective animals at 16 weeks post-reconstitution. (E) Total HSCs in the bone marrow compartment of the respective animals at 16 weeks post-reconstitution. (F) Proportion of bone marrow HSCs expressing Ki-67 in the respective animals at 16 weeks post-reconstitution. Data represents at least two independent experiments and is represented as mean ± SEM. See also Figures S7E–S7H. * denotes $p < 0.05$, ** denotes $p < 0.01$, and *** denotes $p < 0.001$ using a Student's t test.

found that *Mirc19*$^{-/-}$ HSCs had lower amounts of ROS accumulation compared to WT HSCs under conditions of starvation (Figure 7D). The accumulation of ROS was elevated to comparable amounts in WT and *Mirc19*$^{-/-}$ HSCs when autophagy was inhibited with BafA (Figure 7D).

We employed an shRNA silencing strategy for FOXO3 to determine whether it was the key mediator of autophagy in *Mirc19*$^{-/-}$ HSCs. WT and *Mirc19*$^{-/-}$ HSPCs were transduced with either a control vector (MB) or a FOXO3 shRNA construct (shFOXO3) and were subsequently used to reconstitute lethally irradiated WT mice. At 2 months post-reconstitution, we sorted HSCs from these mice and subjected them to the aforementioned assays for autophagy induction and caspase activation under conditions of growth factor starvation. WT HSCs expressing shFOXO3 demonstrated lower autophagy activity and higher amounts of apoptosis compared to WT HSCs expressing MB (Figures 7E and 7F). Importantly, silencing of FOXO3 in *Mirc19*$^{-/-}$ HSCs resulted in a significant reduction in autophagy induction and an increase in caspase activity compared to *Mirc19*$^{-/-}$ HSCs expressing MB. However, this reduction did not reduce autophagy activity completely to that of WT HSCs expressing MB. This might be due to incomplete silencing of FOXO3 in *Mirc19*$^{-/-}$ cells or might suggest factors other than FOXO3 might be involved in mediating autophagy induction (Figures 7E and 7F).

DISCUSSION

MicroRNAs are key regulators of lineage commitment and function in immune cells (Baltimore et al., 2008; Gangaraju and Lin, 2009). Several microRNAs have been implicated in regulating diverse facets of normal HSC maintenance and function, such as cell cycling (Lechman et al., 2012; Song et al., 2013), apoptosis (Guo et al., 2010), engraftment potential (O'Connell et al., 2010), and resistance to inflammatory stress (Zhao et al., 2013). Although much has been done to characterize the functional differences between aged and young HSCs, little is known about how microRNAs might contribute to maintaining balanced hematopoietic output as an organism ages. Our findings suggest that Mirc19, particularly miR-132, is critical in regulating the balance between HSC survival and proliferation and differentiation. We have demonstrated that it does this primarily by buffering the expression of FOXO3 in the aging hematopoietic system. Deregulation of this cluster, and in turn FOXO3, can have negative consequences on the function of HSCs and the output of mature hematopoietic cells, leading to extramedullary hematopoiesis.

Because the expression of miR-132 was higher in HSCs compared to total bone marrow cells, we utilized both gain-of-function and loss-of-function approaches to investigate its role in HSC function and survival. Ectopic expression of miR-132 resulted in hyper-proliferation and depletion of HSCs within the bone marrow compartment. Enforced expression of miR-212 produced a similar but less dramatic phenotype. This depletion of HSCs with miR-132 overexpression coincided with the onset of extramedullary hematopoiesis, including enlarged spleens and fibrotic bone marrow. We observed a drastic decrease in protein expression of the miR-132 target FOXO3 within the bone marrow compartment of miR-132 overexpressing mice. Consistent with our findings, a genetic deletion of *Foxo3* in hematopoietic cells leads to increased HSC proliferation and an

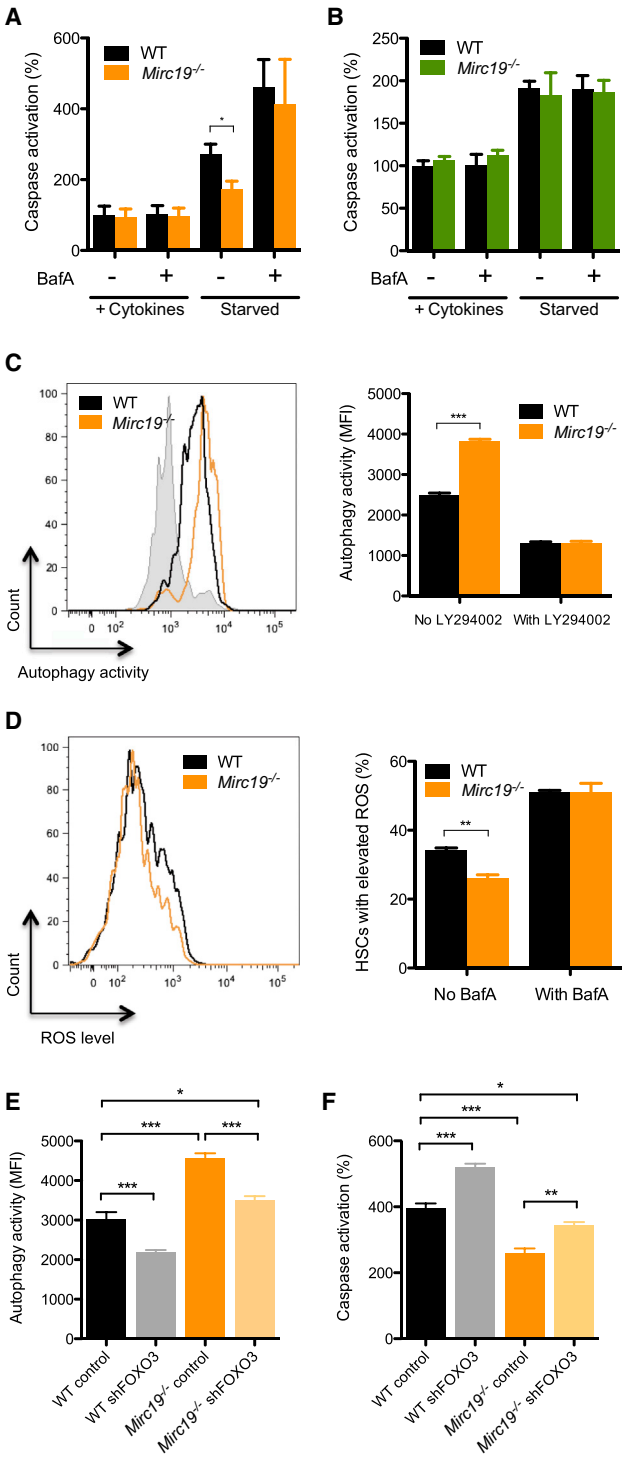

Figure 7. Genetic Deletion of Mirc19 Results in a FOXO3-Dependent Alteration in Autophagy and Survival of HSCs

(A and B) Cells obtained from WT and *Mirc19*$^{-/-}$ mice were cultured with or without growth cytokines (mIL3, mIL6, mSCF, TPO, Flt3L, and G-CSF) or BafA. Caspase activation was measured using a luciferase based assay (n = 6). (A) Caspase activation observed in HSCs from WT and *Mirc19*$^{-/-}$ mice with or without growth factor starvation and BafA treatment. (B) Caspase activation observed in myeloid progenitors from WT and *Mirc19*$^{-/-}$ mice with or without growth factor starvation and BafA treatment.

age-dependent depletion of the HSC pool with loss of HSC long-term reconstitution potential (Miyamoto et al., 2007). This phenotype is exacerbated by the concomitant deletion of the FOXO family members *Foxo1* and *Foxo4* (Tothova et al., 2007). We further found several FOXO3 target genes, particularly the negative cell-cycle regulators p21, p57, and p27, to be downregulated in miR-132 overexpressing bone marrow. Importantly, replenishing expression of FOXO3 during miR-132 overexpression rescued the phenotype we observed.

A genetic deletion of *Mirc19* led to higher basal expression of FOXO3 in bone marrow cells. Over time, this led to a dramatic increase in the number of HSCs, a decrease in production of more committed progenitors, and a defect in HSC cycling in response to environmental stress, such as lipopolysaccharide treatment. Consistent with the more quiescent state of *Mirc19*$^{-/-}$ HSCs, we found they were marginally better at long-term reconstitution of the hematopoietic system than WT counterparts. FOXO3 is a known regulator of apoptosis, and we further demonstrated that ectopic expression of FOXO3 from a retroviral vector resulted in a selection for those cells expressing the lowest amount of the vector, presumably because higher amounts of FOXO3 expression were toxic. We have therefore shown that Mirc19 is important in regulating expression of FOXO3, and that when this target is either upregulated or downregulated, there is a severe alteration in HSC function over time.

The expression of both miR-132 and FOXO3 transcripts is upregulated with age in murine bone marrow cells and early progenitors. The role of FOXO3 as a longevity-associated gene remains unknown in the hematopoietic system. FOXO3 might be upregulated in this context due to its vital role in survival through autophagy and in cell cycling. MicroRNAs play an important role in buffering perturbations in the expression of their targets in response to environmental stress (Ebert and Sharp, 2012). Such stress might include inflammation from repetitive exposure to environmental pathogens and hematopoietic aging. Importantly, the abundance of microRNAs in any given cell plays an important role in establishing a threshold for target expression (Mukherji et al., 2011); as such, upregulation of the microRNA may require higher target expression to maintain important physiological functions. Given that both overexpression and deletion of miR-132 in bone marrow cells led to inappropriate hematopoiesis, we believe that miR-132 plays an important role in buffering FOXO3 protein expression within a defined range to maintain

(C) Autophagy activity in WT and *Mirc19*$^{-/-}$ HSCs with or without growth factor starvation and LY294002 treatment. Autophagy was measured using a dye that fluorescently labels autophagosomes (cyto-ID autophagy assay) (n = 5).
(D) ROS accumulation in WT and *Mirc19*$^{-/-}$ HSCs with or without growth-factor starvation and BafA treatment measured using a fluorescence-based ROS detection system (CellROX assay) (n = 5).
(E and F) WT C57BL/6 mice were lethally irradiated and reconstituted with WT or *Mirc19*$^{-/-}$ donor bone marrow cells expressing either a control or FOXO3 shRNA silencing vector. At 8 weeks post-reconstitution HSCs were sorted from bone marrow and assays were performed. (E) Autophagy activity measured in HSCs from the respective mice in response to growth factor starvation (n = 6). (F) Caspase activation measured in HSCs from the respective mice in response to growth factor starvation (n = 6). Data represents two independent experiments and is represented as mean ± SEM. See also Figure S7I. * denotes $p < 0.05$, ** denotes $p < 0.01$, and *** denotes $p < 0.001$ using a Student's t test.

normal HSC function as an organism ages. The concomitant increase in the expression of miR-132 alongside FOXO3 in the aging hematopoietic system might be critical for maintaining an important balance between known FOXO3-regulated processes, including cell-cycling and differentiation, and apoptosis of HSCs.

The aging hematopoietic system is characterized by an alteration of the balance between self-renewal and differentiation, which leads to the accumulation of less-functional HSCs, myeloid-biased differentiation, and a requirement for basal autophagy for survival (Geiger et al., 2013; Warr et al., 2013). Of note, the loss of critical autophagy factors in the hematopoietic system leads to hyper-proliferation and poor survival of HSCs (Mortensen et al., 2011). Recently, it has also been demonstrated that FOXO3 plays a critical role in inducing protective autophagy of aging HSCs (Warr et al., 2013), which is critical for their survival in response to oxidative stress (Eijkelenboom and Burgering, 2013). The proposed mechanism of FOXO3 regulation of autophagy is through the transcription of glutamine synthase (van der Vos et al., 2012). Consistent with this role of FOXO3 in HSC survival, we found that *Mirc19*$^{-/-}$ HSCs, when compared to WT HSCs, demonstrated increased resistance to growth-factor starvation as evidenced by the decrease in presence of reactive oxygen species, lower amounts of apoptosis induction, and an increase in accumulation of autophagosomes. We observed an abrogation of this effect when we silenced FOXO3 in *Mirc19*$^{-/-}$ HSCs, thus demonstrating that this phenotype is mostly due to the upregulation of FOXO3 in these cells. Importantly, this improved survival of *Mirc19*$^{-/-}$ cells in response to environmental stress might contribute to the age-dependent accumulation of HSCs in *Mirc19*$^{-/-}$ mice compared to WT mice.

Our observations demonstrate that the *Mirc19*$^{-/-}$ cluster is an important regulator of HSC homeostasis by altering cell cycling, function, and survival. This is an example of a microRNA playing a physiological role in maintaining the balance of HSC functions during aging. The capacity of this microRNA to buffer expression of FOXO3 is critical given the multiple roles FOXO3 plays in regulating HSC biology. Our findings open the possibility of utilizing miR-132 mimics or antagonists to alter defects in HSC function that might lead to hematopoietic diseases late in life.

EXPERIMENTAL PROCEDURES

DNA Constructs

For in vivo miR-132 overexpression and FOXO3 shRNA experiments, the mature miR-132 or FOXO3 shRNA sequence was placed in the microRNA-155 loop-and-arms format (O'Connell et al., 2010) and cloned into the MSCV-eGFP (MG) and MSCV-TagBFP (MG) vectors, respectively. For FOXO3 rescue experiments, FOXO3 cDNA was cloned into the MSCV-IRES-eGFP (MIG) vector. See Supplemental Experimental Procedures for more details about these vectors. FOXO3 shRNA target sequences are given in Table S1.

For luciferase assays, the microRNA-132 expression cassette was subcloned into the pCDNA3 vector. The 3′untranslated regions of relevant gene targets containing the miR-132 binding region were cloned immediately downstream of luciferase in the pMiReport vector as previously described (Chaudhuri et al., 2012).

Cell Culture

Cells were cultured in a sterile incubator that was maintained at 37°C and 5% CO_2. 293T cells were cultured in DMEM supplemented with 10% fetal bovine serum, 100 U/mL penicillin and 100 U/mL streptomycin. Primary cells were cultured in complete RPMI supplemented with 10% FBS, 100 U/mL penicillin, 100 U/mL streptomycin, 50 μM β-mercaptoethanol, and appropriate growth cytokines as needed for the experiment.

Cell Sorting for RNA Extraction

For miR-132 expression profiling, bone marrow cells from C57BL/6 mice were depleted of RBCs and sorted for the respective cell populations at the Caltech Flow Cytometry Core Facility. Detailed procedures are provided in the Supplemental Experimental Procedures. RNA was harvested using the miRNAeasy RNA prep kit (QIAGEN). For bone marrow samples from MG and miR-132 mice, bone marrow was harvested from the respective mice, lysed of red blood cells, and spun down. RNA was harvested as described above.

Expression Profiling and qPCR

We performed real time qPCR (RT-qPCR) with a 7300 Real-Time PCR machine (Applied Biosystems) as previously described (Chaudhuri et al., 2012). TaqMan qPCR was performed for miR-132, miR-212, and snoRNA-202 (control) detection as per manufacturer's instructions using TaqMan MicroRNA Assays (Life Technologies). SYBR Green-based RT-qPCR was performed for mRNA of mouse FOXO3, FOXO1, p27, p21, p57, and relevant miR-132 targets following cDNA synthesis using qScript cDNA SuperMix (Quanta) and detection with PerfeCTa qPCR Fastmix with ROX (Quanta) as per manufacturer's instructions. Gene-specific primers used for qPCR are listed in Table S2. RNA-seq library construction and analysis are described in the Supplemental Information.

Target Prediction and Luciferase Reporter Assays

Relevant targets for miR-132 were investigated using predictions from TargetScan Mouse 6.2 software (Friedman et al., 2009) and following sorting by probability of conserved targeting (P_{CT}). Luciferase assays for miR-132 targets were performed as previously described (Chaudhuri et al., 2012). Briefly, 4 × 10^5 cells were plated in 12-well plates for 24 hr and subsequently transfected with either pCDNA or pCDNA-miR-132, a pMiReport vector, and a β-gal expression vector. 48 hr later, cells were lysed using Reporter Lysis Buffer (Promega) and luciferase and β-gal expression was analyzed, respectively, using a Dual Luciferase Kit (Promega) and a chemiluminescent β-gal reporter kit (Roche).

Immunoblotting

Bone marrow samples were prepared as described for RNA preparation. Cell extracts were collected using RIPA lysis buffer (Sigma) and were subjected to gel-electrophoresis and transfer onto a PVDF membrane. Antibody staining was performed using antibodies for FOXO3, p27, and actin. Detailed procedures are given in the Supplemental Information.

Animals

The California Institute of Technology Institutional Animal Care and Use Committee approved all experiments. C57BL/6 WT and miR-212/132$^{-/-}$ mice were bred and housed in the Caltech Office of Laboratory Animal Resources (OLAR) facility. Bone marrow reconstitution experiments were performed as previously described (Chaudhuri et al., 2012) with the aforementioned vectors and are explained in more detail in the Supplemental Experimental Procedures. Recipient mice were monitored for health and peripheral blood was analyzed for mature blood cell types each month up till the experimental end-point at either 16 or 36 weeks post-reconstitution. At each end-point, immune organs were harvested for further analysis as described. The number of mice for each experimental cohort is described in the figure legends. Each experiment was repeated at least twice and, in many cases, three or four times.

Competitive Transplant Experiments

Bone marrow cells from age and gender-matched WT CD45.2$^+$ C57BL/6 mice, *Mirc19*$^{-/-}$ CD45.2$^+$ C57BL/6 mice, and WT CD45.1$^+$ C57BL/6 mice were harvested and depleted of RBCs as described above. A 1:1 ratio of WT CD45.1$^+$ HSCs with either WT or *Mirc19*$^{-/-}$ CD45.2$^+$ HSCs was subsequently injected into lethally irradiated (1,000 rads) WT CD45.2$^+$ CD57BL/6 mice. Mice were monitored for up to 20 weeks post-reconstitution and relevant tissues were harvested for further analysis by flow cytometry.

Flow Cytometry

Relevant tissues were harvested and cells were homogenized and subsequently depleted of red blood cells as described above. Flurophore-conjugated antibodies were used for the indicated markers, and detected using a MACSQuant10 Flow Cytometry machine (Miltenyi). Detailed procedures are given in the Supplemental Information.

Autophagy and Reactive-Oxygen Species Assays

HSCs were sorted as described above from either WT or *Mirc19*$^{-/-}$ C57BL/6 mice, or from reconstituted mice with donor WT or *Mirc19*$^{-/-}$ bone marrow infected with either MB or shFOXO3 retroviral constructs. Cells were then cultured with the appropriate growth factors and cytokines, or authophagy inhibitors, and processed for caspase activity (Promega), the presence of ROS (Life Technologies), or autophagy activity (Enzo Life Sciences). Detailed procedures are given in the Supplemental Information.

Statistical Tests

All statistical analysis was done in Graphpad Prism software using an unpaired Student's t test. Data were reported as mean ± SEM. Significance measurements were marked as follows: * $p < 0.05$, ** $p < 0.01$, ** $p < 0.001$, or ns for not significant.

ACCESSION NUMBER

The RNA-seq data used in this study can be accessed from the Gene Expression Omnibus under the accession project ID GSE66352.

SUPPLEMENTAL INFORMATION

Supplemental Information includes three figures, two tables, and Supplemental Experimental Procedures and can be found with this article online at http://dx.doi.org/10.1016/j.immuni.2015.05.017.

AUTHOR CONTRIBUTIONS

A.M., J.L.Z., and D.B. designed the study. A.M. conducted all the experimental work with assistance from N.S., M.M., M.S.K., R.P.G, and X.D. and with guidance from J.L.Z. G.K.M. and A.M. performed bioinformatics analysis. E.E. and K.C. contributed the *Mirc19*$^{-/-}$ mice. A.M. and D.B. wrote the manuscript with contributions from all authors.

ACKNOWLEDGMENTS

We thank Diana Perez at the Caltech Flow Cytometry core facility, and Igor Antoshechkin and Vijaya Kumar at the Caltech Genetics and Genomics Laboratory for their assistance. We also thank Michael T. Bethune for helpful discussions throughout the preparation of this manuscript. This work was supported by an NIH RO1AI079243 (D.B.), National Research Service Award CA183220 (A.M.), HL110691 (J.L.Z.), the UCLA/Caltech Medical Scientist Training Program (A.M. and J.L.Z.), the Human Frontiers Science Foundation (M.M.), and the Broad Institute (M.S.K. and A.R.).

Received: December 28, 2014
Revised: February 28, 2015
Accepted: May 20, 2015
Published: June 16, 2015

REFERENCES

Baltimore, D., Boldin, M.P., O'Connell, R.M., Rao, D.S., and Taganov, K.D. (2008). MicroRNAs: new regulators of immune cell development and function. Nat. Immunol. *9*, 839–845.

Chaudhuri, A.A., So, A.Y., Mehta, A., Minisandram, A., Sinha, N., Jonsson, V.D., Rao, D.S., O'Connell, R.M., and Baltimore, D. (2012). Oncomir miR-125b regulates hematopoiesis by targeting the gene Lin28A. Proc. Natl. Acad. Sci. USA *109*, 4233–4238.

Chen, C.Z., Li, L., Lodish, H.F., and Bartel, D.P. (2004). MicroRNAs modulate hematopoietic lineage differentiation. Science *303*, 83–86.

Ebert, M.S., and Sharp, P.A. (2012). Roles for microRNAs in conferring robustness to biological processes. Cell *149*, 515–524.

Eijkelenboom, A., and Burgering, B.M. (2013). FOXOs: signalling integrators for homeostasis maintenance. Nat. Rev. Mol. Cell Biol. *14*, 83–97.

Esplin, B.L., Shimazu, T., Welner, R.S., Garrett, K.P., Nie, L., Zhang, Q., Humphrey, M.B., Yang, Q., Borghesi, L.A., and Kincade, P.W. (2011). Chronic exposure to a TLR ligand injures hematopoietic stem cells. Journal of immunology (Baltimore, Md.: 1950) *186*, 5367-5375.

Filipowicz, W., Bhattacharyya, S.N., and Sonenberg, N. (2008). Mechanisms of post-transcriptional regulation by microRNAs: are the answers in sight? Nat. Rev. Genet. *9*, 102–114.

Flach, J., Bakker, S.T., Mohrin, M., Conroy, P.C., Pietras, E.M., Reynaud, D., Alvarez, S., Diolaiti, M.E., Ugarte, F., Forsberg, E.C., et al. (2014). Replication stress is a potent driver of functional decline in ageing haematopoietic stem cells. Nature *512*, 198–202.

Frasca, D., and Blomberg, B.B. (2011). Aging affects human B cell responses. J. Clin. Immunol. *31*, 430–435.

Friedman, R.C., Farh, K.K., Burge, C.B., and Bartel, D.P. (2009). Most mammalian mRNAs are conserved targets of microRNAs. Genome Res. *19*, 92–105.

Gangaraju, V.K., and Lin, H. (2009). MicroRNAs: key regulators of stem cells. Nat. Rev. Mol. Cell Biol. *10*, 116–125.

Geiger, H., de Haan, G., and Florian, M.C. (2013). The ageing haematopoietic stem cell compartment. Nat. Rev. Immunol. *13*, 376–389.

Guo, S., Lu, J., Schlanger, R., Zhang, H., Wang, J.Y., Fox, M.C., Purton, L.E., Fleming, H.H., Cobb, B., Merkenschlager, M., et al. (2010). MicroRNA miR-125a controls hematopoietic stem cell number. Proc. Natl. Acad. Sci. USA *107*, 14229–14234.

Henry, C.J., Marusyk, A., and DeGregori, J. (2011). Aging-associated changes in hematopoiesis and leukemogenesis: what's the connection? Aging (Albany, N.Y. Online) *3*, 643–656.

Lagos, D., Pollara, G., Henderson, S., Gratrix, F., Fabani, M., Milne, R.S., Gotch, F., and Boshoff, C. (2010). miR-132 regulates antiviral innate immunity through suppression of the p300 transcriptional co-activator. Nat. Cell Biol. *12*, 513–519.

Lechman, E.R., Gentner, B., van Galen, P., Giustacchini, A., Saini, M., Boccalatte, F.E., Hiramatsu, H., Restuccia, U., Bachi, A., Voisin, V., et al. (2012). Attenuation of miR-126 activity expands HSC in vivo without exhaustion. Cell Stem Cell *11*, 799–811.

Miyamoto, K., Araki, K.Y., Naka, K., Arai, F., Takubo, K., Yamazaki, S., Matsuoka, S., Miyamoto, T., Ito, K., Ohmura, M., et al. (2007). Foxo3a is essential for maintenance of the hematopoietic stem cell pool. Cell Stem Cell *1*, 101–112.

Mortensen, M., Soilleux, E.J., Djordjevic, G., Tripp, R., Lutteropp, M., Sadighi-Akha, E., Stranks, A.J., Glanville, J., Knight, S., Jacobsen, S.E., et al. (2011). The autophagy protein Atg7 is essential for hematopoietic stem cell maintenance. J. Exp. Med. *208*, 455–467.

Mukherji, S., Ebert, M.S., Zheng, G.X., Tsang, J.S., Sharp, P.A., and van Oudenaarden, A. (2011). MicroRNAs can generate thresholds in target gene expression. Nat. Genet. *43*, 854–859.

Nakahama, T., Hanieh, H., Nguyen, N.T., Chinen, I., Ripley, B., Millrine, D., Lee, S., Nyati, K.K., Dubey, P.K., Chowdhury, K., et al. (2013). Aryl hydrocarbon receptor-mediated induction of the microRNA-132/212 cluster promotes interleukin-17-producing T-helper cell differentiation. Proc. Natl. Acad. Sci. USA *110*, 11964–11969.

Ni, B., Rajaram, M.V., Lafuse, W.P., Landes, M.B., and Schlesinger, L.S. (2014). Mycobacterium tuberculosis decreases human macrophage IFN-gamma responsiveness through miR-132 and miR-26a. Journal of immunology *193*, 4537–4547.

Novershtern, N., Subramanian, A., Lawton, L.N., Mak, R.H., Haining, W.N., McConkey, M.E., Habib, N., Yosef, N., Chang, C.Y., Shay, T., et al. (2011). Densely interconnected transcriptional circuits control cell states in human hematopoiesis. Cell *144*, 296–309.

O'Connell, R.M., Chaudhuri, A.A., Rao, D.S., Gibson, W.S., Balazs, A.B., and Baltimore, D. (2010). MicroRNAs enriched in hematopoietic stem cells differentially regulate long-term hematopoietic output. Proc. Natl. Acad. Sci. USA *107*, 14235–14240.

Orkin, S.H., and Zon, L.I. (2008). Hematopoiesis: an evolving paradigm for stem cell biology. Cell *132*, 631–644.

Passegué, E., Wagers, A.J., Giuriato, S., Anderson, W.C., and Weissman, I.L. (2005). Global analysis of proliferation and cell cycle gene expression in the regulation of hematopoietic stem and progenitor cell fates. J. Exp. Med. *202*, 1599–1611.

Pietras, E.M., Warr, M.R., and Passegué, E. (2011). Cell cycle regulation in hematopoietic stem cells. J. Cell Biol. *195*, 709–720.

Rossi, L., Lin, K.K., Boles, N.C., Yang, L., King, K.Y., Jeong, M., Mayle, A., and Goodell, M.A. (2012). Less is more: unveiling the functional core of hematopoietic stem cells through knockout mice. Cell Stem Cell *11*, 302–317.

Rubinsztein, D.C., Mariño, G., and Kroemer, G. (2011). Autophagy and aging. Cell *146*, 682–695.

Shaked, I., Meerson, A., Wolf, Y., Avni, R., Greenberg, D., Gilboa-Geffen, A., and Soreq, H. (2009). MicroRNA-132 potentiates cholinergic anti-inflammatory signaling by targeting acetylcholinesterase. Immunity *31*, 965–973.

Song, S.J., Ito, K., Ala, U., Kats, L., Webster, K., Sun, S.M., Jongen-Lavrencic, M., Manova-Todorova, K., Teruya-Feldstein, J., Avigan, D.E., et al. (2013). The oncogenic microRNA miR-22 targets the TET2 tumor suppressor to promote hematopoietic stem cell self-renewal and transformation. Cell Stem Cell *13*, 87–101.

Strovas, T.J., Rosenberg, A.B., Kuypers, B.E., Muscat, R.A., and Seelig, G. (2014). MicroRNA-based single-gene circuits buffer protein synthesis rates against perturbations. ACS synthetic biology *3*, 324–331.

Suda, T., Takubo, K., and Semenza, G.L. (2011). Metabolic regulation of hematopoietic stem cells in the hypoxic niche. Cell Stem Cell *9*, 298–310.

Sun, D., Luo, M., Jeong, M., Rodriguez, B., Xia, Z., Hannah, R., Wang, H., Le, T., Faull, K.F., Chen, R., et al. (2014). Epigenomic profiling of young and aged HSCs reveals concerted changes during aging that reinforce self-renewal. Cell Stem Cell *14*, 673–688.

Tothova, Z., Kollipara, R., Huntly, B.J., Lee, B.H., Castrillon, D.H., Cullen, D.E., McDowell, E.P., Lazo-Kallanian, S., Williams, I.R., Sears, C., et al. (2007). FoxOs are critical mediators of hematopoietic stem cell resistance to physiologic oxidative stress. Cell *128*, 325–339.

Ucar, A., Gupta, S.K., Fiedler, J., Erikci, E., Kardasinski, M., Batkai, S., Dangwal, S., Kumarswamy, R., Bang, C., Holzmann, A., et al. (2012). The miRNA-212/132 family regulates both cardiac hypertrophy and cardiomyocyte autophagy. Nat. Commun. *3*, 1078.

van der Vos, K.E., Eliasson, P., Proikas-Cezanne, T., Vervoort, S.J., van Boxtel, R., Putker, M., van Zutphen, I.J., Mauthe, M., Zellmer, S., Pals, C., et al. (2012). Modulation of glutamine metabolism by the PI(3)K-PKB-FOXO network regulates autophagy. Nat. Cell Biol. *14*, 829–837.

Warr, M.R., Binnewies, M., Flach, J., Reynaud, D., Garg, T., Malhotra, R., Debnath, J., and Passegué, E. (2013). FOXO3A directs a protective autophagy program in haematopoietic stem cells. Nature *494*, 323–327.

Willcox, B.J., Donlon, T.A., He, Q., Chen, R., Grove, J.S., Yano, K., Masaki, K.H., Willcox, D.C., Rodriguez, B., and Curb, J.D. (2008). FOXO3A genotype is strongly associated with human longevity. Proc. Natl. Acad. Sci. USA *105*, 13987–13992.

Zhao, J.L., Rao, D.S., O'Connell, R.M., Garcia-Flores, Y., and Baltimore, D. (2013). MicroRNA-146a acts as a guardian of the quality and longevity of hematopoietic stem cells in mice. eLife *2*, e00537.

Immunity

Supplemental Information

The MicroRNA-132 and MicroRNA-212 Cluster Regulates Hematopoietic Stem Cell Maintenance and Survival with Age by Buffering FOXO3 Expression

Arnav Mehta, Jimmy L. Zhao, Nikita Sinha, Georgi K. Marinov, Mati Mann, Monika S. Kowalczyk Rachel P. Galimidi, Xiaomi Du, Erdem Erikci, Aviv Regev, Kamal Chowdhury, David Baltimore

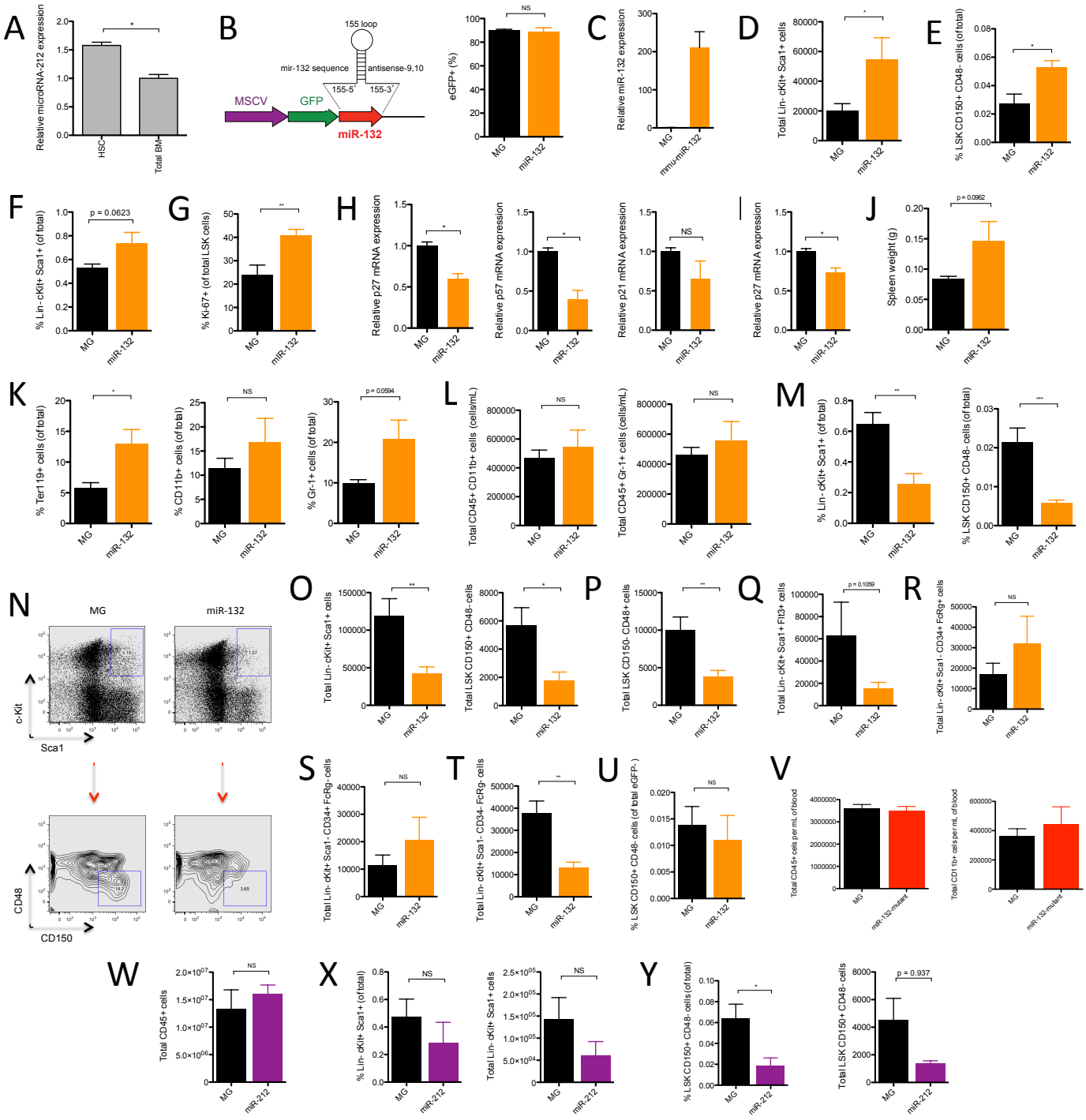
A
Relative microRNA-212 expression
HSC
Total BM
B
155 loop
mir-132 sequence
antisense-9,10
155-5'
155-3'
MSCV
GFP
miR-132
eGFP+ (%)
NS
MG
miR-132
C
Relative miR-132 expression
mmu-miR-132
D
Total Lin- cKit+ Sca1+ cells
E
% LSK CD150+ CD48- cells (of total)
F
% Lin- cKit+ Sca1+ (of total)
p = 0.0623
G
% KI-67+ (of total LSK cells)
H
Relative p27 mRNA expression
Relative p57 mRNA expression
Relative p21 mRNA expression
Relative p27 mRNA expression
J
Spleen weight (g)
p = 0.0952
K
% Ter119+ cells (of total)
% CD11b+ cells (of total)
p = 0.0594
% Gr-1+ cells (of total)
L
Total CD45+ CD11b+ cells (cells/mL)
Total CD45+ Gr-1+ cells (cells/mL)
M
% Lin- cKit+ Sca1+ (of total)
% LSK CD150+ CD48- cells (of total)
N
MG
miR-132
c-Kit
Sca1
CD48
CD150
O
Total Lin- cKit+ Sca1+ cells
Total LSK CD150+ CD48- cells
P
Total LSK CD150- CD48+ cells
Q
Total Lin- cKit+ Sca1+ Flt3+ cells
p = 0.1059
R
Total Lin- cKit+ Sca1- CD34+ FcRg+ cells
S
Total Lin- cKit+ Sca1- CD34+ FcRg- cells
T
Total Lin- cKit+ Sca1- CD34- FcRg- cells
U
% LSK CD150+ CD48- cells (of total eGFP-)
V
Total CD45+ cells per mL of blood
miR-132-mutant
Total CD11b+ cells per mL of blood
W
Total CD45+ cells
miR-212
X
% Lin- cKit+ Sca1+ (of total)
Total Lin- cKit+ Sca1+ cells
Y
% LSK CD150+ CD48- cells (of total)
Total LSK CD150+ CD48- cells
p = 0.937

Figure S1, related to Figure 1: Ectopic expression of microRNA-132 leads to dregulated hematopoiesis. (A) miR-212 expression in total bone marrow and HSCs. (B) Schematic of the retroviral construct used to over-express miR-132 and reconstitution efficiency of mice transplanted with MG or miR-132 donor bone marrow. Peripheral blood was analyzed at 8-weeks post-reconstitution for the proportion of eGFP+ CD45+ leukocytes. (C) Expression of miR-132 in bone marrow cells obtained from MG and miR-132 mice. Data is represented as mean ± SEM. (D) – (U) WT C57BL/6 mice were lethally irradiated and reconstituted with donor bone marrow cells expressing either a control (MG) or a miR-132 over-expressing (miR-132) retroviral vector (n=8-12 mice per group). Data represents at least three independent experiments and is shown for 16-weeks post-reconstitution unless otherwise specified. (D) Total number of LSK cells in the bone marrow at 8-weeks post-reconstitution. (E) Frequency of HSCs in the bone marrow at 8-weeks post-reconstitution. (F) Frequency of LSK cells in the bone marrow at 8-weeks post-reconstitution. (G) Percentage of Ki-67+ cells within the bone marrow LSK at 8-weeks post-reconstitution. (H) p27, p57, and p21 transcript expression in the bone marrow at 2-months post-reconstitution. (I) p27 transcript expression in the bone marrow compartment at 4-months post-reconstitution. (J) Spleen weights. (K) Percentage of Ter119+, CD11b+ and Gr-1+ cells in the spleen. (L) Total number of CD11b+ and Gr-1+ cells in the peripheral blood. (M) Representative FACS plot and gating for HSCs (Lineage- Sca1+ cKit+ CD150+ CD48-). (N) Percentage of LSK cells and HSCs in the bone marrow. (O) Total number of LSK cells and HSCs at 9-months post-reconstitution. Total number of (P) multipotent progenitors (MPPs), (Q) lymphoid primed MPPs (LMPPs), (R) granulocyte-monocyte progenitors (GMPs), (S) common myeloid

progenitors (CMPs), and (T) myeloid-erythroid progenitors (MEPs) in the bone marrow. (U) Percentage of HSCs in the bone marrow within the eGFP- population. (V) WT C57BL/6 mice were lethally irradiated and reconstituted with donor bone marrow cells expressing either a control (MG) or a miR-132-mutant over-expressing (miR-132-mutant) retroviral vector in which the miR-132 seed sequence was mutated (n=5 mice per group). Graphs show total peripheral blood CD45+ leukccytes and CD11b+ cells at 9-months post-reconstitution. (W) – (Y) WT C57BL/6 mice were lethally irradiated and reconstituted with donor bone marrow cells expressing either a control (MG) or a miR-212 over-expressing (miR-212) retroviral vector (n=4 mice per group). (W) Total bone marrow CD45+ cells. (X) Frequency and total number of LSK cells in the bone marrow. (Y) Frequency and total number of HSCs in the bone marrow. Data is represented as mean ± SEM. * denotes $p < 0.05$, ** denotes $p < 0.01$ and *** denotes $p < 0.001$ using a Student's *t* test.

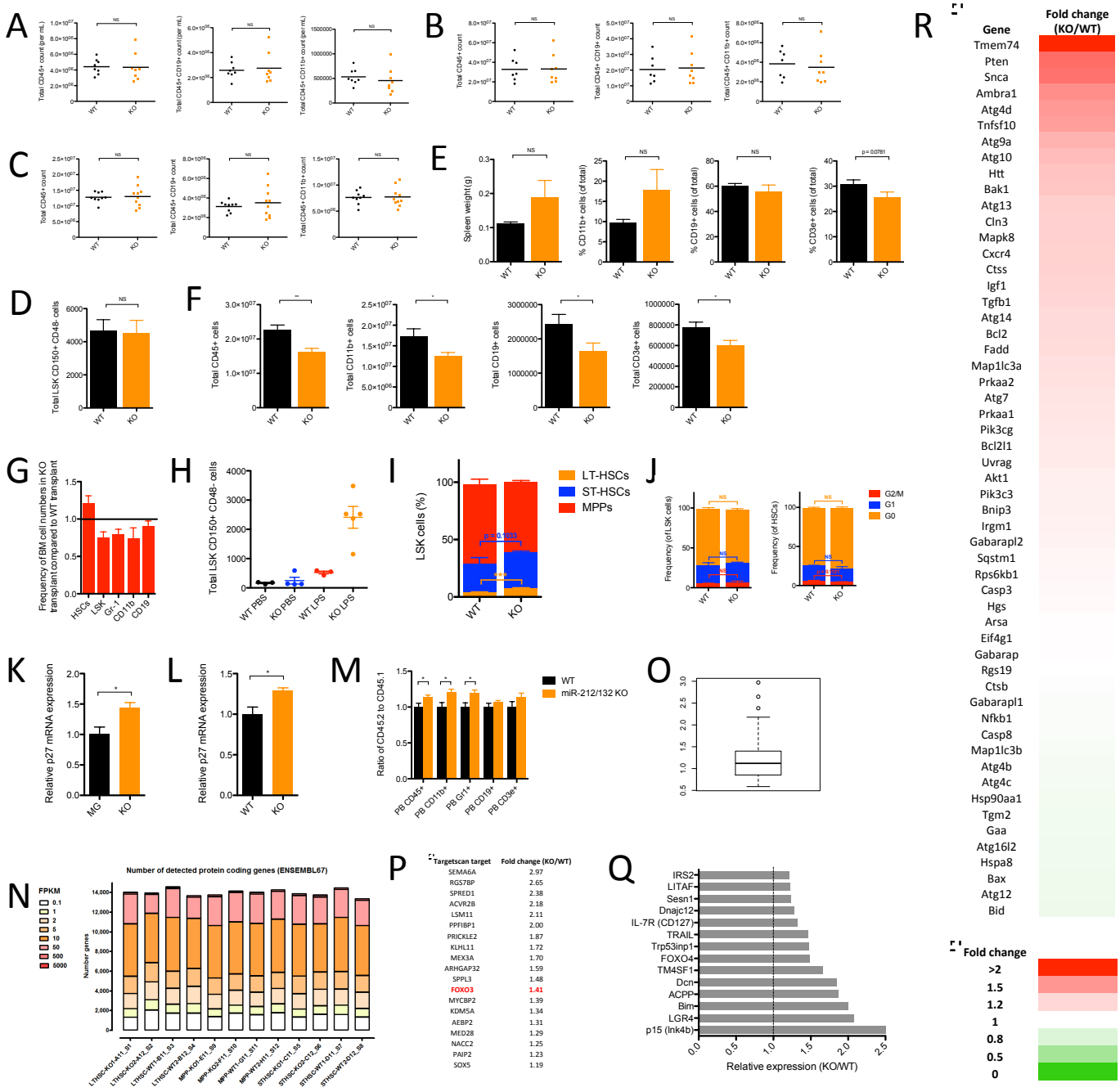
A
B
C
D
E
F
G
Frequency of BM cell numbers in KO transplant compared to WT transplant
HSCs
LSK
Gr-1
CD11b
CD19
H
Total LSK CD150+ CD48- cells
WT PBS
KO PBS
WT LPS
KO LPS
I
LSK cells (%)
LT-HSCs
ST-HSCs
MPPs
J
Frequency (of LSK cells)
Frequency (of HSCs)
G2/M
G1
G0
K
Relative p27 mRNA expression
L
M
Ratio of CD45.2 to CD45.1
WT
miR-212/132 KO
PB CD45+
PB CD11b+
PB Gr1+
PB CD19+
PB CD3e+
O
N
Number of detected protein coding genes (ENSEMBL67)
FPKM
Number genes
P
Targetscan target
Fold change (KO/WT)
SEMA6A 2.97
RGS7BP 2.65
SPRED1 2.38
ACVR2B 2.18
LSM11 2.11
PPFIBP1 2.00
PRICKLE2 1.87
KLHL11 1.72
MEX3A 1.70
ARHGAP32 1.59
SPPL3 1.48
FOXO3 1.41
MYCBP2 1.39
KDM5A 1.34
AEBP2 1.31
MED28 1.29
NACC2 1.25
PAIP2 1.23
SOX5 1.19
Q
IRS2
LITAF
Sesn1
Dnajc12
IL-7R (CD127)
TRAIL
Trp53inp1
FOXO4
TM4SF1
Dcn
ACPP
Bim
LGR4
p15 (Ink4b)
Relative expression (KO/WT)
R
Gene
Fold change (KO/WT)
Tmem74
Pten
Snca
Ambra1
Atg4d
Tnfsf10
Atg9a
Atg10
Htt
Bak1
Atg13
Cln3
Mapk8
Cxcr4
Ctss
Igf1
Tgfb1
Atg14
Bcl2
Fadd
Map1lc3a
Prkaa2
Atg7
Prkaa1
Pik3cg
Bcl2l1
Uvrag
Akt1
Pik3c3
Bnip3
Irgm1
Gabarapl2
Sqstm1
Rps6kb1
Casp3
Hgs
Arsa
Eif4g1
Gabarap
Rgs19
Ctsb
Gabarapl1
Nfkb1
Casp8
Map1lc3b
Atg4b
Atg4c
Hsp90aa1
Tgm2
Gaa
Atg16l2
Hspa8
Bax
Atg12
Bid
Fold change
>2
1.5
1.2
1
0.8
0.5
0

Figure S2, related to Figures 2 and 3: Genetic deletion of Mirc19 in mice leads to deregulated hematopoiesis with age. (A) – (C) Mice with a genetic deletion of Mirc19 (*Mirc19*$^{-/-}$) along with WT mice in the C57BL/6 background were analyzed to understand the physiological contribution of Mirc19 on hematopoietic output (n=7-8 mice per group). (A) Total number of peripheral blood CD45+, CD19+ and CD11b+ cells at 12-weeks of age. (B) Total number of splenic CD45+, CD19+ and CD11b+ cells at 12-weeks of age. (C) Total number of bone marrow CD45+, CD19+ and CD11b+ cells at 12-weeks of age. (D) Total number of HSCs in the bone marrow at 12-weeks of age. (E) Spleen weight, and percentage of splenic CD11b+, CD19+ and CD3e+ cells at 60-64 weeks of age. (F) Total number of CD45+, CD11b+, CD19+ and CD3e+ cells in the bone marrow at 60-64 weeks of age. (G) WT or *Mirc19*$^{-/-}$ (KO) bone marrow cells were transplanted into lethally irradiated C57BL/6 mice. The relative ratio (KO/WT) of total numbers of various cell populations in the bone marrow of these mice at 60-weeks post-reconstitution is shown. (H) – (J) 6-month old WT and *Mirc19*$^{-/-}$ mice were treated with 9 evenly-spaced low-dose (1mg/kg of body weight) LPS or PBS injections over one month. (H) Total number of HSCs in the spleen. (I) Relative proportions of early progenitors in the bone marrow. (J) Proportion of bone marrow LSK cells and HSCs in each stage of the cell cycle (G0, G1, G2/M). (K) Expression of p27 in the bone marrow compartment. (L) Expression of p27 in the bone marrow compartment of mice 5-days after a single treatment of 5-fluorouracil. (M) WT or *Mirc19*$^{-/-}$ CD45.2+ bone marrow cells from primary transplant experiments, calibrated for the total number of phenotypically defined HSCs, were injected in a 1:1 ratio with CD45.1+ WT bone marrow cells into irradiated C57BL/6 CD45.2+ recipients. The graph represents the relative ratio of mature cells in

the peripheral blood of these secondary transplant mice at 16-weeks post-reconstitution. (O) Summary of the number of detected protein coding genes and FPKM values for sequenced samples. LT-HSC: long-term HSCs, LSK CD150+ CD48-. SH-HSCs: short-term HSCs, LSK CD150- CD48-. MPPs: multipotent progenitors, LSK CD150- CD48+. WT: wildtype sample. KO: *Mirc19*$^{-/-}$ sample. (O) Box-plot showing enrichment of miR-132 targets in miR-212/132$^{-/-}$ HSCs compared to WT HSCs. (P) Fold-change of several miR-132 targets in miR-212/132$^{-/-}$ HSCs compared to WT HSCs. (Q) Fold-change in several FOXO3 regulated genes in miR-212/132$^{-/-}$ HSCs compared to WT HSCs. (R) Fold-change in several autophagy related genes in miR-212/132$^{-/-}$ HSCs Data represents at least two independent experiments and is represented as mean ± SEM. * denotes $p < 0.05$, ** denotes $p < 0.01$ and *** denotes $p < 0.001$ using a Student-T test.

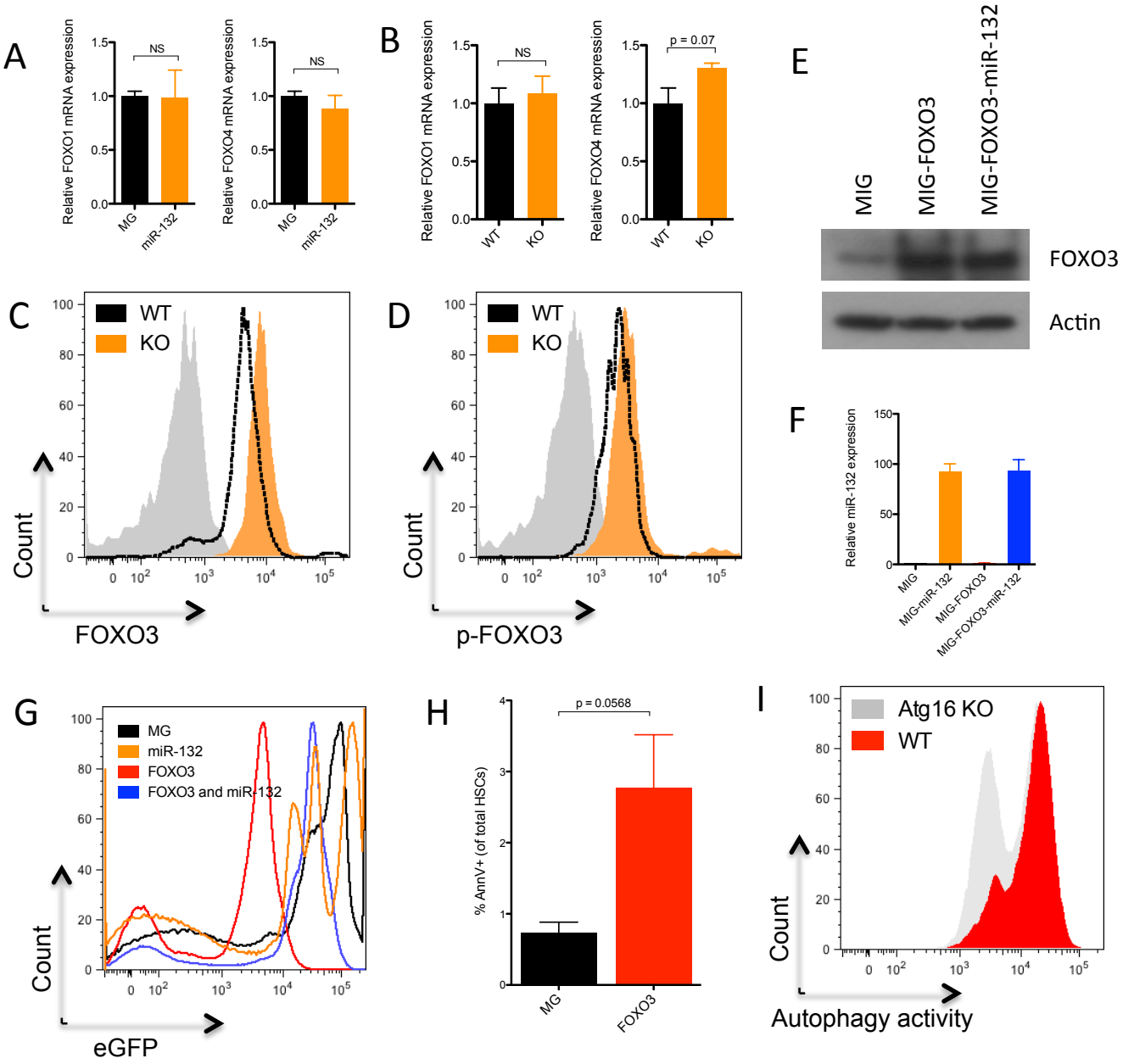
A
Relative FOXO1 mRNA expression
NS
MG
miR-132
Relative FOXO4 mRNA expression
NS
MG
miR-132
B
Relative FOXO1 mRNA expression
NS
WT
KO
Relative FOXO4 mRNA expression
p = 0.07
WT
KO
E
MIG
MIG-FOXO3
MIG-FOXO3-miR-132
FOXO3
Actin
C
WT
KO
Count
FOXO3
D
WT
KO
Count
p-FOXO3
F
Relative miR-132 expression
MIG
MIG-miR-132
MIG-FOXO3
MIG-FOXO3-miR-132
G
MG
miR-132
FOXO3
FOXO3 and miR-132
Count
eGFP
H
p = 0.0568
% AnnV+ (of total HSCs)
MG
FOXO3
I
Atg16 KO
WT
Count
Autophagy activity

Figure S3, related to Figures 6 and 7: Validation of microRNA-132 and FOXO3 over-expression in FOXO3 rescue experiment. (A) FOXO1 and FOXO4 expression in total bone marrow cells from WT^{MG} and $WT^{miR-132}$ mice. (B) FOXO1 and FOXO4 expression in lineage-depleted bone marrow cells from WT and miR-212/132$^{-/-}$ mice. RNA was obtained from the respective cell populations and FOXO1 and FOXO4 expression was quantified by RT-qPCR (n=2-3 biological replicates). (C) Intracellular staining analyzed by FACS for FOXO3 protein expression in bone marrow HSCs obtained from WT and miR-212/132$^{-/-}$ mice and starved for 12 hours *in-vitro*. (D) Intracellular staining analyzed by FACS for phosphorylated FOXO3 (p-FOXO3) protein expression in bone marrow HSCs obtained from WT and miR-212/132$^{-/-}$ mice and starved for 12 hours *in-vitro*. (E) – (F) Bone marrow expressing either a control (MIG), a miR-132 over-expressing (MIG-miR-132), a FOXO3 over-expressing (MIG-FOXO3), or a FOXO3 and miR-132 over-expressing (MIG-FOXO3-miR-132) retroviral vector were analyzed using Taqman RT-qPCR for miR-132 expression or Western Blot for FOXO3 protein expression. (E) FOXO3 protein expression in bone marrow cells transduced with the indicated retroviral vectors. (F) Mature miR-132 expression in in bone marrow cells transduced with the indicated retroviral vectors. (G) eGFP expression in the bone marrow compartment of mice reconstitution with bone marrow cells transduced with the indicated retroviral vector. (H) AnnexinV staining performed on bone marrow HSCs from MIG and MIG-FOXO3 mice (n=3). (I) Detection of autophagy activity using the Cyto-ID autophagy detection assay in bone-marrow-derived dendritic cells treated with Rapamycin and obtained from WT and Atg16 deficient (Atg16 KO) mice. Data represents at least two independent experiments and is represented as mean ± SEM.

Supplemental Experimental Procedures

DNA Constructs

The miR-132 over-expression construct was cloned into the MSCV-eGFP (MG) vector. In this modified vector, MG-miR-132, containing an MSCV promoter, the eGFP is placed immediately downstream of the 5' LTR and the miR-132 expression cassette is placed immediately downstream of the eGFP stop codon. A miR-132-mutant vector was similar constructed with a mutated miR-132 seed sequence. For FOXO3 rescue experiments, FOXO3 cDNA was cloned into the MSCV-IRES-eGFP (MIG) vector, immediately downstream of the 5' LTR and upstream of the IRES. miR-132 was cloned downstream of eGFP as described above. For FOXO3 knockdown experiments, TagBFP was first subcloned into the MG vector, creating MSCV-TagBFP (MB). Several FOXO3 shRNA sequences were designed using the Invitrogen Block-iT RNAi Designer and cloned in the microRNA-155 loop-and-arms format immediately downstream of TagBFP in the MB vector.

Cell sorting for RNA extraction

Bone marrow cells were harvested from WT C57BL/6 mice and depleted of red blood cells (RBCs) using RBC lysis buffer (BioLegend). Cells were then spun down, resuspended in MACS separating buffer (Phosphate buffered saline, pH7.2, with 0.5% BSA and 2mM EDTA) and filtered through a 70uM cell-strainer. These cells were then blocked with FcBlock (Becton Dickinson) and depleted of mature cells on a magnetic column using biotin-conjugated mouse antibodies for CD3e, CD8, CD4, CD19, B220, CD11b, Gr-1, IL-7Ra, and Ter119 (BioLegend) and streptavidin magnetic beads

(Miltenyi), as suggested by the manufacturer (Miltenyi). Cells were subsequently stained with fluorophore-conjugated antibodies for lineage markers (CD3, CD19, CD11b, Gr-1, Ter119, Nk1.1), cKit, Sca1, CD150, CD48 and with 7-AAD, and several populations were sorted for analysis including HSCs (Lineage- cKit+ Sca1+ CD150+ CD48-), LSK cells (Lineage- cKit+ Sca1+), and other progenitor subsets as detailed in the text. Cells were sorted on a FACSAria IIu cell sorter (Becton Dickinson) at the Caltech Flow Cytometry Core Facility. Mature cell populations were sorted using a magnetic column as described above using positive-selection for the respective surface marker (Gr-1, CD11b, CD19). All cells were lysed using Qiazol lysis buffer (Qiagen) and processed using the miRNAeasy RNA prep kit (Qiagen). RNA was then subjected to qPCR.

Sample preparation for RNA-sequencing

LT-HSCs (LSK CD150+ CD48-), ST-HSCs (LSK CD150- CD48-) and MPPs (LSK CD150- CD48+) from WT and miR-212/132$^{-/-}$ were sorted as described above. Cells were sorted directly into cell lysis buffer and processed using an RNAeasy kit (Qiagen) with *DNAseI* digestion (Qiagen) as per manufacturer's protocol. Libraries were prepared using the SMART-seq2 protocol (Picelli et al., 2013) modified to use Maxima H Minus enzyme for reverse transcription (Thermo Scientific) (Satija et al., 2015). Amplified cDNA products were purified using AMPure XP SPRI beads (Beckman Coulter) and eluted in TE buffer (Teknova). Cleaned-up amplified cDNA was used for library construction using the Nextera XT DNA Sample Preparation Kit and Nextera XT Index Kit (Illumina). Libraries were then pooled and cleaned-up using AMPure XP SPRI beads

(Beckman Coulter Genomics). Final library quality and quantity were assessed using a DNA High Sensitivity chip (Agilent).

RNA-seq data generation and analysis

Libraries were sequenced on the Illumina HiSeq 2500. Paired-end 2x25bp reads were generated. The reads were filtered for rRNA contamination by aligning against mouse ribosomal sequences using Bowtie (version 0.12.7) (Langmead et al., 2009), and retaining unaligned read pairs. The refSeq annotation for the mm9 version of the mouse genome was used to create a transcriptome Bowtie index, to which read pairs were aligned with the following settings: "-v 2 -a -X 1000". Gene expression levels were estimated using eXpress (version 1.5.1) (Roberts and Pachter, 2013), and the effective count values were used as input to DESeq (Anders and Huber, 2010) for evaluating differential expression. The targets of miR-132 were obtained from TargetScan (mouse release 6.2) (Friedman et al., 2009).

Immunoblotting

Pelleted cells were resuspended in RIPA lysis buffer (Sigma) containing protease inhibitors for 20 minutes on ice. Samples were spun down at max speed at 4^{o}C for 10 minutes and the supernatant was processed immediately or flash-frozen on dry ice for analysis in the future. Total cell extracts were fractionated by gel-electrophoresis on a mini-PROTEAN TGX gradient (4-15%) gel (Bio-Rad) and electroblotted onto a PVDF membrane using a wet transfer apparatus (Bio-Rad). Protein detection was subsequently performed with the following antibodies: FoxO3a (75D8) (Cell Signaling Technologies),

p27-HRP (sc-538) (Santa Cruz Biotechnology), actin-HRP (sc-1616) (Santa Cruz Biotechnology) and goat anti-rabbit-IgG-HRP (sc-2030) (Santa Cruz Biotechnology).

Mice

All mice used in this study are of the C57BL/6 background. The miR-212/132$^{-/-}$ mice were generated previously and are described elsewhere (Ucar et al., 2012). Briefly, these mice were generated by homologous recombination targeting the genomic cluster containing both microRNA-212 and microRNA-132. Mice obtained were backcrossed to the C57BL/6 background for at least 20 generations prior to the initiation of the reported studies.

Bone marrow reconstitution

WT C57BL/6 or miR-212/132$^{-/-}$ mice were treated with 5-fluorouracil (10ug; Sigma) for 5 days to enrich for hematopoietic stem and progenitor cells (HSPCs) in the bone marrow. After 5 days, bone marrow cells were harvested, red blood cells (RBCs) were lysed with RBC lysis buffer (BioLegend), and cells were plated in HSPC media which was comprised of complete RPMI with mouse SCF (50 ng/mL), IL-3 (20 ng/mL), and IL-6 (50 ng/mL). Cells were then cultured in 24-wel plates for 24 hours and spin-infected with PCL-ecotropic pseudotyped gamma-retrovirus expressing the construct of interest, which was either a microRNA, shRNA or a gene, as described in under the *DNA Constructs and Primers* section of the main text. Spin-infections were performed by removing supernatant carefully from cell culture plates and adding virus with 8 ug/mL Polybrene (Santa Cruz Biotechnology). Plates

were then placed in a centrifuge for 2 hours at 30^0C and 2500RPM. Immediately following infection, virus supernatant was removed and replaced with HSPC media. 24 hours later a second identical spin infection was performed. After another 24 hours, recipient mice were lethally irradiated (1000 rads from Cs137 source) and 250,000 to a million virus-infected HSPCs were retro-orbitally delivered to reconstitute the immune system. Recipients were maintained on Septra and in autoclaved cages for at least one month post-reconstitution.

Virus production

To generate retrovirus for HSPC infection, 10 million HEK293T cells were first plated in a 15cm plate. 24 hours later, cells were transfected with both the pCL-Eco vector and either the pMG vector or the relevant variant described above for gene delivery. For transfection, we used BioT (Bioland Scientific) as per the manufacturers protocol. 36 hours after transfection, virus was collected, filtered through a 45uM syringe filter, and used for infection of HSPCs.

Flow cytometry

Cells were stained with fluorophore-conjugated antibodies (all from BioLegend unless indicated) for CD45.1, CD45.2, CD11b, Gr-1, CD19, B220, CD3e, Nk1.1, Ter119, cKit, Sca1, CD150, CD48, EPCR (Ebioscience), CD34, Flt3, FcRg or IL-7Ra in various combinations to characterize relevant hematopoietic cell populations. Intracellular staining was performed by first performing surface staining of cells, followed by fixation and permeabilization (Cytofix/Cytoperm kit; BD Biosciences) and subsequent staining

with either Ki67 (BioLegend) and Hoescht33342 (Life Technologies) for cell-cycling analysis, or an anti-FoxO3a (75D8) (Cell Signaling Technologies) or anti-FoxO3a (phosphor S253) (Abcam) primary antibody followed by an anti-Rabit-IgG secondary antibody conjugated to Alexafuor488 (Cell Signaling Technologies). Samples were analyzed on a MACSQuant10 Flow Cytometry machine (Miltenyi). Gating and analysis was performed using FlowJo software.

Autophagy and reactive-oxygen species assays

HSCs were sorted as described above from either WT or miR-212/132$^{-/-}$ C57BL/6 mice, or from reconstituted mice with donor WT or miR-212/132$^{-/-}$ bone marrow infected with either MB or shFOXO3 retroviral constructs. For all in-vitro experiments, cells were sorted directly in a 96-wel plate containing cell culture media with the appropriate growth factors and cytokines (all from Ebioscience). For caspase activation assays and reactive oxygen species detection, 5000 cells were cultured with or without Bafilomycin A (5nM; Sigma) and with either no growth factors or cytokines, or with mSCF (50 ng/mL), IL-3 (20 ng/mL), IL-6 (50 ng/mL), Flt3L (25 ng/mL), TPO (25 ng/mL), and GM-CSF (10ng/mL). Cells were cultured for 12 hours and subsequently processed. Caspase activity was detected using the luciferase-based Caspase Glo 3/7 assay system as per manufactures instructions (Promega). Reactive-oxygen species were detected by flow cytometry using the CellROX Deep Red reagent (Life Technologies). For authophagy detection assays, 5000-8000 cells were cultured with or without LY294002 (20uM; Cell Signaling Technologies) and with or without aforementioned growth factors or cytokines.

Autophagy activity was determined by flow cytometry using the CytoID autophagy detection kit as per manufacturers instructions (Enzo Life Sciences).

Table S1, related to *DNA Constructs* in Experimental Procedures. Sequences for FOXO3 shRNA constructs. These sequences were cloned into the MSCV-eGFP retroviral vector to silence FOXO3 expression in bone marrow cells.

FOXO3 shRNA sequence (in miR-155-arms-and-loop-format)	
mmu-FOXO3 shRNA #1	gaaggctgtaTGCTGCCATCATTCAGATTCATGGTGGTTTTGGCCACTGACTGACCACCATGACTGAATGATGGcaggacacaaggcctg
mmu-FOXO3 shRNA #2	gaaggctgtaTGCTGAACACGGTACTGTTGAAGGAGGTTTTGGCCACTGACTGACCTCCTTCAAGTACCGTGTTcaggacacaaggcctg
mmu-FOXO3 shRNA #3	gaaggctgtaTGCTGAAGAGAAGGTGGCTGGTCTGTGTTTTGGCCACTGACTGACACAGACCACACCTTCTCTTcaggacacaaggcctg

Table S2, related to *Expression profiling and qPCR* in Experimental Procedures.

Primer sequences used for qPCR to quantify expression of various genes. These forward (F) and reverse (R) primers were used to quantify mRNA expression of various genes using RT-qPCR.

Primer sequences

AchE F	CTCCCTGGTATCCCCTGCATA
AchE R	GGATGCCCAGAAAAGCTGAGA
BTG2 F	ATGAGCCACGGGAAGAGAAC
BTG2 R	GCCCTACTGAAAACCTTGAGTC
FOXO1 F	CCCAGGCCGGAGTTTAACC
FOXO1 R	GTTGCTCATAAAGTCGGTGCT
FOXO3 F	CTGGGGGAACCTGTCCTATG
FOXO3 R	TCATTCTGAACGCGCATGAAG
HMGA2 F	GAGCCCTCTCCTAAGAGACCC
HMGA2 R	TTGGCCGTTTTTCTCCAATGG
JARID1A F	CACAGACCCGCTGAGTTTTAT
JARID1A R	CTTCACAGGCAAATGGAGGTT
Lin28b F	AGAATGCAGTCTACCTCCTCAG
Lin28b R	CCTCCCACTTCTCTTGGTGC
MAPK1 F	GGTTGTTCCCAAATGCTGACT
MAPK1 R	CAACTTCAATCCTCTTGTGAGGG
MMP9 F	CTGGACAGCCAGACACTAAAG
MMP9 R	CTCGCGGCAAGTCTTCAGAG
p21 F	CCGCTGGAGGGCAACTTCGT
p21 R	TTTCGGCCCTGAGATGTTCC
p27 F	TCTCAGGCAAACTCTGAGGAC
p27 R	TTCGGAGCTGTTTACGTCTGG
p300 F	CTCGCACTTGCCCTTACCTTT
p300 R	GGTCGCAGTGGCTGGAGA
p57 F	TGATGAGCTGGGAACTGAGCC
p57 R	ACGTCGTTCGACGCCTTGTTC
PTBP2 F	GGATCTGACGAGCTACTCTCA
PTBP2 R	TTCTTACTATCGTTACCGTTGGC
RB1 F	TGCATCTTTATCGCAGCAGTT
RB1 R	GTTCACACGTCCGTTCTAATTTG
SOX4 F	GACAGCGACAAGATTCCGTTC
SOX4 R	GTTGCCCGACTTCACCTTC
SOX5 F	CCCGTGATCCAGAGCACTTAC
SOX5 R	CCGCAATGTGGTTTTCGCT

Supplemental References

Anders, S., and Huber, W. (2010). Differential expression analysis for sequence count data. Genome Biol *11*, R106.

Friedman, R.C., Farh, K.K., Burge, C.B., and Bartel, D.P. (2009). Most mammalian mRNAs are conserved targets of microRNAs. Genome Res *19*, 92-105.

Langmead, B., Trapnell, C., Pop, M., and Salzberg, S.L. (2009). Ultrafast and memory-efficient alignment of short DNA sequences to the human genome. Genome Biol *10*, R25.

Picelli, S., Bjorklund, A.K., Faridani, O.R., Sagasser, S., Winberg, G., and Sandberg, R. (2013). Smart-seq2 for sensitive full-length transcriptome profiling in single cells. Nat Methods *10*, 1096-1098.

Roberts, A., and Pachter, L. (2013). Streaming fragment assignment for real-time analysis of sequencing experiments. Nat Methods *10*, 71-73.

Satija, R., Farrell, J.A., Gennert, D., Schier, A.F., and Regev, A. (2015). Spatial reconstruction of single-cell gene expression data. Nature biotechnology.

Ucar, A., Gupta, S.K., Fiedler, J., Erikci, E., Kardasinski, M., Batkai, S., Dangwal, S., Kumarswamy, R., Bang, C., Holzmann, A.*, et al.* (2012). The miRNA-212/132 family regulates both cardiac hypertrophy and cardiomyocyte autophagy. Nat Commun *3*, 1078.